Cooperativity among clustered κB sites within promoters and enhancers dictates transcriptional specificity of NF-κB-RelA along with specific cofactors

Shandy Shahabi[1], Tapan Biswas[1], Yuting Shen[1], Rose Sanahmadi[1], Yaya Zou[1], and Gourisankar Ghosh[1,5]

[1]Department of Chemistry and Biochemistry, University of California San Diego, 9500 Gilman Drive, La Jolla, CA 92093, USA

Running Title: clustered κB sites and cofactors in DNA recognition by NF-κB RelA

[5]To whom correspondence should be addressed: Dr. Gourisankar Ghosh, Department of Chemistry and Biochemistry, University of California San Diego, 9500 Gilman Drive, La Jolla, California 92093, USA, Telephone: 858-822-0469; E-mail: gghosh@ucsd.edu

Keywords: NF-kappa B (NF-κB), transcription, κB DNA, cofactor, promoter

ABSTRACT

The functional role of weak DNA binding sites for transcription factor (TF) recruitment and gene expression remains largely unknown. Our study reveals that the weak NF-κB DNA binding sites, which are abundant in gene promoters and enhancers, appear in clusters and exhibit minimal to undetectable NF-κB binding activity in isolation in vitro, yet they play prominent roles in gene regulation within native context in cells. We found nuclear concentration of RelA/p65, the predominant NF-κB, is approximately 0.2 μM in stimulated cells, challenging the idea that these weak κB sites operate through mass action-dependent binding mechanisms. Through proteomic analysis, we identified a range of nuclear factors, including various other TFs, interacting with RelA at these κB-sites. ChIP-seq, RNA-seq and phase-separated condensation analyses suggest these additional TFs, referred to as the cofactors of NF-κB, facilitate dynamic recruitment of NF-κB to clustered κB sites of specific target genes. Overall, our findings demonstrate the collective contribution of both strong and weak κB sites in occupancy of NF-κB at the promoters and enhancers, with the recruitment facilitated by a variety of cofactors. This congregation of multiple factors forming larger dynamic complexes appearing as a transcription condensate is likely to be common to all transcriptional programs.

INTRODUCTION

Transcriptional regulation is mediated by transcription factors (TFs) that bind specifically to short DNA response elements (REs) located within the non-coding regions known as promoter and enhancer (Lambert et al., 2018; Todeschini et al., 2014). Over the past decade, genome-wide and imaging analyses have immensely contributed to our understanding of interactions between TFs and their REs of eukaryotic protein-coding genes (Farnung and Vos, 2022; Kim and Wysocka, 2023; Meeussen and Lenstra, 2024). However, these studies have also highlighted unresolved fundamental questions about how sequence-specific DNA recognition by transcription factors is achieved in cells (Badis et al., 2009; Kim and Wysocka, 2023; Zuin et al., 2022). Among these, two intriguing aspects related to transcription factors (TFs) engaging the gene regulatory region that have remained unresolved are the following: First, the presence of multiple TF binding sites with a wide range of affinities raises the question of whether weak binding sites play a role in transcription, which has not been systematically addressed. Second, many TFs are found associated with the enhancer and promoter regions lacking their cognate DNA binding sites, hinting at non-DNA binding roles of these TFs in gene expression. Whether auxiliary TFs facilitate DNA-binding TF to the weak site has also remained unknown. We address these questions using transcriptional programs mediated by NF-κB RelA, a suitable model system due to rigorous studies on it over decades.

Among the NF-κB family of TF dimers, the p50:RelA heterodimer and the RelA:RelA homodimer are most ubiquitous and best studied (Ghosh et al., 2012; Mulero et al., 2019). These dimers bind with high-affinity to ~10-bp sequences (κB sites), with a general consensus of GGGRNNYYCC, defined over 35 years ago (Lenardo and Baltimore, 1989). However, natural promoters exhibit an array of diverse κB sites (Mulero *et al.*, 2019; Siggers et al., 2011), some of which are not easily recognizable. Consistently, Siggers et al. have analyzed the binding of thousands of degenerate κB sites to various NF-κB dimers and discovered that these putative sites exhibited a gradient of weak but variable binding to these dimers. Several of these weak binding sites corresponded to sequences within the promoters of known NF-κB target genes, though the functional role of the vast majority of these sites remains unknown. A few promoters of NF-κB regulated genes such as E-selectin, Cxcl10, Ccl2, IL-1β, TNFα, and Nfkbia have been characterized in greater detail. They all contain multiple κB sites with some binding to NF-κB dimers with lower affinity. Cell-based reporter assays indicated the necessity of these weak sites in optimal reporter expression (Mulero et al., 2017; Mulero *et al.*, 2019). However, the prevalence of weak κB sites in these and other native promoters and enhancers is not known. Similarly, the lower limits of binding affinity of weak κB sites to be functional have not been properly defined.

The weak DNA binding sites of various transcription factors within the enhancer regions have also been demonstrated to play essential roles during development (Crocker et al., 2015; Crocker et al., 2016; Farley et al., 2015; Kribelbauer et al., 2019; Lim et al., 2024); where suboptimal binding of TFs to these weak sites appears to provide specificity of gene expression. Lim et al. have shown that even a small enhancement of binding affinity from 15% to 25% relative to the strongest binding due to a natural single nucleotide change, of a binding site for the TF, ETS, becomes pathogenic (Lim *et al.*,

2024). However, the biochemical mechanism of how several binding sites within an enhancer collectively function remains unclear.

Previous studies have also revealed another property of NF-κB; it is often recruited along with additional factors (Fu et al., 2013; Mulero et al., 2018; Mulero *et al.*, 2019; Wan et al., 2007). However, the mechanism of how these factors facilitate DNA binding remains unknown, except these studies indicated promoter, subunit, and cell type specificity of these auxiliary factors in RelA recruitment. Even with these discoveries, mechanisms of how these factors assist in the interaction between RelA and promoter are not known. Importantly, these properties are not exclusive to NF-κB. Other TFs have also been shown to bind a variety of DNA sites and require auxiliary factors for DNA recognition.

Given the importance of these unresolved issues in transcription, we set out to investigate how NF-κB binds DNA and activates transcription, focusing on weak κB sites and the role of supporting factors. We investigated stimulus-dependent expression of genes by NF-κB p50:RelA and RelA:RelA dimers and found that κB sites are present in clusters within ~150 DNA segments of promoters and enhancers. Our findings indicate that weak κB sites, that show minimal to no binding in vitro, play essential roles in recruiting NF-κB and driving transcription of target genes. Additionally, we show that numerous protein factors, referred to here as cofactors, including other TFs, RNA proteins, and enzymes, associate with NF-κB RelA on DNA. Further investigation of these TF-cofactors reveals their importance in enhancer/promoter specific recruitment of RelA.

RESULTS

Clustered κB sites with wide range of affinities are present in promoters of NF-κB target genes and they collectively dictate RelA recruitment to DNA

We examined the relationship between ChIP-seq scores of RelA, representing its occupancy to DNA in the cell, and sequence of κB sites within the promoters of over 100 NF-κB-regulated genes that are stimulated by TNFα within a 30-minute stimulation period, as reported by Ngo et al (Ngo et al., 2020). The sites are designated as κB sites if they matched any of the 1800 sites with a measurable Z-score derived from PBM analysis (Siggers *et al.*, 2011). These κB sites display a maximum deviation at three positions from the 10-bp consensus. Notably, we observed the presence of multiple weak κB sites surrounding a strong κB site within a 500 bp window centered around the ChIP-seq peak for most TNFα-responsive genes (**Figure 1A**). These promoters can be separated based on their cumulative RelA Z-scores. The top and bottom promoters of ranked genes show a significant difference in terms of the number of κB sites (**Figure 1B**). The ChIP-seq peak aligned to a strong κB site in nearly all cases. Intriguingly, we observed only a weak correlation between the ChIP-seq score and Z-score of the strong κB site (**Supplementary Figure 1A**). This suggests that the affinity of an individual strong site is insufficient in dictating occupancy of RelA dimers to promoter regions in cells. However, we observed a stronger correlation of ChIP-seq strength to the number of probable κB sites surrounding the ChIP-seq peak site (**Figure 1C**).

Although we analyzed a window of 500 bp around the peak, clusters of κB sites spanned mostly about 200 bp, which is similar to the span of open chromatin observed within promoters and enhancers during transcription (**Figure 1C** and **Supplementary Figure 1A**). We further analyzed the arrangement of κB sites in promoters of Cxcl1, Cxcl2, Nfkbid, and Tnfaip3 (**Figure 1D** and **Supplementary Figure 1B**). Both Cxcl1 and Cxcl2 share an identical strong site (GGGAAATTCC) but the Cxcl2 promoter displayed a lower overall ChIP score compared to Cxcl1. This may be a reflection of the Cxcl1 promoter containing a higher number of weak κB sites than Cxcl2 (13 vs 8), and the cumulative Z-score of its weak sites for RelA dimers is also higher than that of Cxcl2 (70.6 vs 58.5). Some of these weak sites exhibiting minimal resemblance to the κB consensus, such as GGA<u>T</u>TTT<u>TT</u> and GGGAATTT<u>TA</u> (deviation from consensus underlined), are found near the strong site in Cxcl1 and Tnfaip3 promoters. To assess if these putative weak sites engage to RelA dimers, we measured affinities of selected κB sites for both NF-κB RelA homodimer and p50:RelA heterodimer (of wild-type full-length proteins) at a near-physiological salt concentration by biolayer interferometry (BLI) assays. Both NF-κB dimers bound these putative sites with a much-reduced affinity when compared with binding to IFN-α: GGGAAATTCC, and IFN-γ: GGGAAGTTCC sites as references of strong and weak κB sites. For most weak sites, the K_d could not be determined accurately, although minor binding was detected at higher protein concentrations. Two sites did not display any affinity even at the highest protein concentration (**Figure 1E** and **Supplementary Figure 1C**) and estimated to have K_d >1500 nM. Since the nuclear concentration of RelA upon TNFα stimulation is around 230 nM as determined here (**Supplementary Figure 1D**), only about 6% of these dimers are expected to bind at a K_d of 3000 nM. These findings raised questions on the authenticity and functional relevance of these putative sites

in vivo. Another important aspect is the mismatch between binding constants measured with native proteins at near physiological ionic strengths using solution-based methods and truncated proteins under non-physiological ionic strength using microarray-based assay. Furthermore, we qualitatively examined the binding strengths of weak and strong sites within Cxcl1 and Cxcl2 promoters using EMSA (**Supplementary Figure 1E**). EMSA with weak and strong sites within Cxcl1 and Cxcl2 promoters indicated that mutation of both κB sites (M5) abrogated binding of NF-κB, while sequence-specific binding at weak κB sites (M4) was retained upon mutation of strong sites. These findings led us to conclude that these two weak sites are indeed putative κB sites as they both displayed weak binding under low salt (i.e., EMSA) conditions.

To evaluate the authenticity of specific binding by NF-κB dimers to weak κB sites, we crystallized the homodimer of RelA in complex with a weak κB site ($^{-5}G^{-4}G^{-3}G^{-2}\underline{C^{-1}T^{0}}T^{+1}T^{+2}T^{+3}C^{+4}C$) present in the promoter of the Cxcl2 gene (the underlined bp are non-cognate and ^{0}T bp denotes the pseudo-dyad axis separating the two DNA half sites). Remarkably, the crystal structure revealed a similar binding interaction as observed with consensus κB sites (**Figure 1F**). The Arg33 and Arg35 engaged the $^{-4}G^{-3}G$ of half-sites as predicted. However, the presence of non-cognate $^{-2}C^{-1}T$ compared to $^{-2}A^{-1}A$ (cognate bp for the RelA subunit) influences the global DNA architecture such that Arg187 is slightly differently positioned, but more importantly, the R41 could not engage with ^{-5}G of the weak site. This altered protein-DNA contact corroborated weaker affinity, but nonetheless indicates specific binding. In summary, these results reveal specific functional involvement of weak κB sites within clusters found in promoters of NF-κB regulated genes.

Weak sites within κB clusters drive NF-κB-induced transcription

We investigated the potential of weak κB sites in transcriptional activation of target genes in cellular milieu. Using CRISPR, we selectively deleted strong and its neighboring weak κB sites, independently, in the promoters of five NF-κB target genes — Cxcl1, Cxcl2, Nfkbid, Map3k8, and Tnfaip3 (**Figure 2A**). A control was also established by deleting a random segment away from any κB site. Sequencing of bulk populations revealed deletions averaging around 4-10 bp (**Supplementary Figure 2A**). These pooled lines were grown, and the transcript levels of target genes were measured by quantitative PCR (qPCR) upon treatment with TNFα (10 ng/ml) for 1 h. We observed a significantly reduced level of transcript in all tested genes upon deletion of both the strong and weak sites (**Figure 2B and Supplementary Figure 2B**). The weak sites of different genes were different in sequence, orientation, and relative distance from the strong site. Chromatin immunoprecipitation (ChIP) assays using a specific antibody against RelA with the wild-type and mutated Cxcl2 promoters indicated a significant reduction of RelA ChIP signal upon deletion of κB sites, weak or strong, compared to the control site deletion (**Figure 2C**). These results support the critical function of weak sites in NF-κB RelA recruitment and transcription.

To further validate the authenticity and role of these weak sites in transcription, we constructed luciferase reporters containing promoter segments of Cxcl1 and Cxcl2 genes (as used in EMSA). Consistent with what was observed in the native context, mutation of either the strong or the weak site

led to a drastic reduction in reporter expression. This indicates that the presence of both κB sites of Cxcl1 or Cxcl2 promoters is critical for optimal reporter expression i.e., a functional synergy between the sites in activating transcription (**Figure 2D**). To explore the synergy between multiple κB sites further, we assessed reporter expression from synthetic promoters containing combinations of strong and weak κB sites with different spacing and orientations. We not only observed two sites to act synergistically but also observed a strikingly robust reporter activity from two weak sites as observed with two strong sites (**Figure 2E**). Reporter activity decreased progressively as the spacing between the sites increased to 100 bp. Overall, these observations suggest a strong activating influence of clustered κB sites, even if weak, in gene activation – outperforming a single strong site.

A multitude of nuclear proteins associate with signal induced NF-κB bound to κB DNA

The apparent weakness of κB sites found in promoter regions of RelA regulated genes raises the question not only about their authenticity but also about the presence of other hidden cooperative or synergistic processes leading to effective recruitment of RelA dimers to these sites in vivo. The abundance of a multitude of nuclear factors congregating with the nucleosome indicates the possibility of additional nuclear factors influencing recruitment of RelA in cells. We explored this with a simplistic strategy of pulldown of factors from nuclear extracts of TNFα-stimulated MEF cells with Cxcl2 promoter DNA fragment as described earlier for EMSA and reporter expression assay. First, we confirmed the specificity of pull-down by testing binding of RelA to the wild-type (WT) but not to the mutant (M5) promoter fragment via Western blotting (**Supplementary Figure 3A**). Subsequently, we incubated with DNA with MEF cell nuclear extract post- 0.5 and 3 h stimulation with TNFα, and performed mass-spectrometry analysis of associated proteins. The difference between WT and M5 (both κB sites are deleted) DNA served in selecting RelA-κB-site specific proteins, and we identified several nuclear proteins (**Figure 3A**, **Supplementary Table 1**) that included other transcription factors (TFs), DNA repair proteins, RNA-binding proteins, and metabolic enzymes. Among the TFs, various members of the NFAT family were prominent, and members of TEAD, SMAD, and CUX families were also represented. RNA binding proteins belonging to the SR family splicing factors and hnRNPs were also abundant.

To investigate the possible uniqueness of nuclear factors associating with RelA bound to either specific promoters or at different times post-induction, we performed pulldown experiments also with Ccl2 promoter DNA fragments using nuclear extracts of MEF cells 0.5 and 3 h post-TNFα stimulation (**Figure 3A**). A largely similar set of proteins engaged to Cxcl2 and Ccl2 DNA fragments, with the exception of a few promoter-specific factors. However, factors associated were markedly different at 0.5 h vs 3 h post-TNFα stimulation, suggesting temporal specificity. Pathway analysis of pulled down proteins revealed transcriptional regulation, NF-κB signaling, and NFAT signaling among the most significantly enriched pathways (**Figure 3B**).

Further investigation using bone marrow-derived macrophage (BMDM) cells treated or untreated with LPS for 1 h corroborated these findings. Notably, NFAT factors pulled down with NF-κB in TNFa-treated MEFs were also identified in LPS-treated BMDM pulldowns. Three main protein

classes were consistently identified: DNA-binding TFs, RNA-binding proteins, and various enzymes (**Figure 3C** and **Supplementary Table 1**). Additionally, we observe the NF-κB and NFAT family members identified under different pulldown conditions (**Figure 3D**). In all pulldown experiments, we also identified a large number of proteins bound to all DNAs under all conditions, indicating they were bound non-specifically.

We focused on five TFs, Nfatc1, Nfat5, Tead3, Cux1, and Smad4, that have their own transcriptional programs by binding to specific DNA sequences. In this case, we set out to investigate if these factors play a role in RelA's recruitment to specific promoters and induction of transcription. We first tested if these TFs interact with RelA. To elucidate their interaction between RelA, we co-expressed them as FLAG-fusion proteins with HA-tagged RelA, followed by co-immunoprecipitation in HEK 293T (**Supplementary Figure 3B**). Results indicated association between RelA and all five factors to various extents, suggesting their potential roles in sequestering RelA in the nucleus or supporting its DNA binding. Among these proteins, Nfatc1 interacts with RelA strongest and is able to pulldown endogenous RelA efficiently (**Supplementary Figure 3C**). Moreover, Nfatc1 appeared to localize in the nucleus along with RelA in response to TNFa (**Supplementary Figure 3D**). Using purified p50:RelA heterodimer, Flag-Nfatc1, and Flag-Tead3, we also observe that Nfatc1 and Tead3 can bind with sequence specificity to the Cxcl2 promoter DNA at overlapping regions of p50:RelA, supporting the potential for their association with NF-κB on DNA (**Supplemental Figure 3E**). We term these RelA-interacting TFs as "TF-cofactors (TF-CoFs)," and propose that they, along with other identified factors, collectively facilitate RelA recruitment to promoters containing κB sites. In essence, we identified numerous cofactors temporally associating with RelA and potentially other NF-κB factors on promoter DNA fragments harboring κB sites.

TF-cofactors support the promoter recruitment of NF-κB RelA

To assess the role of cofactors in regulating DNA binding by NF-κB RelA, we investigated whether RelA's binding to the κB sites is influenced by these five TF-cofactors: Nfatc1, Nfat5, Tead3, Cux1 and Smad4. Knockdown (KD) cell lines for Nfatc1, Nfat5, Tead3, Cux1, and Smad4 were generated using shRNA directed towards each cofactor in MEFs. Scrambled KD (scr-KD) MEF cells were used as the WT control. KD efficiency was validated by measuring protein levels, showing a reduction of approximately 60-80% compared to scr-KD control cells (**Supplementary Figure 4A**).

To examine how the TF-CoFs affect the genome-wide binding pattern of RelA, we performed chromatin immunoprecipitation followed by sequencing (ChIP-seq) with a RelA-specific antibody at TNF stimulation of 0 and 30 min in scr-KD and five TF-CoF KD MEFs (**Figure 4A**). Bioinformatic analysis of the replicate datasets (p-value < 1E-5) identified 9096 RelA peaks that were TNF-inducible at 30 m in these samples (**Figure 4B**, left). Consistent with previous reports, most of the RelA binding sites in scr-KD cells were in intergenic regions (40.9%) or gene bodies, with only a small percentage (~11%) in the promoter region (defined as -1 kb to +100 bp of the TSS) (**Figure 4B**, right). In each KD MEF line, defects in RelA binding were observed in many promoters, but binding was also enhanced in some cases. Analysis of overall RelA binding at RelA-induced peaks revealed that Nfat5 and Cux1

depletion had the greatest defects in RelA recruitment, followed by Nfatc1 and Smad4 (**Figure 4C**, **Supplemental Figure 4B**). RelA binding was reduced only to a few promoters upon Tead3 depletion. Interestingly, to a significant fraction, Tead3 depletion enhanced RelA recruitment suggesting Tead3 acts as a repressor of RelA. Nfatc1 and Nfat5 depletion exhibited a common pattern of RelA recruitment change suggesting they work together. Normalized RelA ChIP-seq density over all identified peaks clearly showed Tead3 had minimal effect, Cux1 had maximal effect, and the rest fell in between. Overall, a significant portion of RelA binding sites were affected in at least one of the KD cells, with only a few promoters affected by all five KDs. Genome browser tracks of two known NF-κB target genes, *Rgs19 and Ccl8*, present peaks that were high in scr-KD cells that become reduced in both Nfatc1 and Nfat5 KD cells, but not in Cux1 KD cells. However, we observe reduced binding at CD44 promoter upon Cux1 KD (**Supplementary Figure 4C**). Further, we observe that NF-κB from TNF-stimulated nuclear extract of Nfatc1-KD cells binds less to Cxcl2 promoter DNA relative to control scr-KD nuclear extract (**Supplemental Figure 4D**).

Since the chosen cofactors are all DNA-binding TFs, we investigated if they influence RelA's DNA binding by binding to their own DNA response elements near or overlapping a κB site. Motif analysis revealed that consensus κB sites were the primary TF binding sites (log p-value = -2.8E4) in control scr-KD MEFs (**Figure 4D**). Except for Tead3, the consensus sequences of other cofactors were not enriched at cross-linked sites. However, given the overlap between Tead3, Nfats, and NF-κB binding sites, it's challenging to ascertain if these factors bind directly to κB sites. Hence, we focused on Cux1 and Smad4 binding sites and found no enrichment of their DNA binding sites near RelA/NF-κB binding sites. This suggests that cofactors primarily, if not exclusively, act through protein-protein interactions rather than direct DNA binding. Overall, these results suggest that each of the tested cofactors supports RelA recruitment only to a select set of promoters, but also impacts negatively on other promoters.

TF-cofactors regulate gene expression by RelA

To determine if reduced levels of these five TF-cofactors and altered RelA recruitment to promoters correlate with transcript levels of genes that are regulated by RelA, we treated all five cell types used in the ChIP experiments, as well as scramble-KD control MEFs with TNFa for 1 hr, followed by genome-wide bulk RNA sequencing. The RNA isolated from untreated cells served as controls. RNA-seq analysis of triplicate samples identified hundreds of genes that were differentially expressed in these five cell types when compared to control cells (p-value < 0.05; **Figure 5A**). The heatmaps display transcript levels in scr-KD (WT) and five KD cells, with genes arranged from highest to lowest expression in induced scr-KD cells (Figure 5A). Unlike the shared RelA ChIP pattern between the Nfat family members, expression patterns did not strongly match. Interestingly, Smad4-KD cells exhibited expression defects in the largest number of genes, despite their unremarkable role in RelA recruitment compared to the other cofactors. Tead3 KD cells showed higher transcript levels for many genes with higher RelA ChIP scores. Examples of affected genes by knockdown of all five factors are shown in **Figure 5B**. Expression of most of the cytokine genes was impacted by one or more of these TF-CoFs

tested. IL6 expression was affected by all five KD cells, whereas Nfkbia was not by any of them. Each KD affected distinct, common, and combinatorial sets of genes, suggesting that RelA-regulated promoters follow distinct rules.

We then sought to understand the correlation between transcript levels and ChIP-seq scores for each KD. Excluding Tead3, we found that reduced ChIP scores generally correlated with reduced transcript levels in the other four cases (**Figure 5C and Supplementary Figure 5A**). As shown in figure 5C, a greater number of genes (105/209) with reduced ChIP-seq score also had lower transcript levels in Nfatc1 KD cells. However, some genes showed higher transcript levels despite higher (20/209) or lower (15/209) ChIP-seq scores. Nfatc1 KD also enhanced ChIP scores of several genes (89/206), of which 20/89 showed higher expression. In some of these cases, the lack of correlation may be due to direct binding of the TF-CoFs to promoters acting as legitimate TFs by antagonizing RelA binding and imposing their own transcriptional regulation patterns. This was evident in Tead3-KD MEFs where more promoters exhibited higher RelA ChIP scores and transcript levels consistent with its repressor activity by binding to cognate DNA motifs (**Figure 5C**). We next examined whether KD of these cofactors affected gene clusters with common biological functions but found no specific biological functions for these cofactors. Overall, we found a lack of correlation between RelA ChIP and transcript levels in control or any KD cells except for a set of genes under KD conditions, which is consistent with previous reports as RNA levels are strongly influenced by other factors post-transcriptionally (Ngo *et al.*, 2020). These results imply a complex relationship between TF-CoFs and RelA in terms of RelA recruitment, subsequent transcription, and perhaps post-transcription.

Clustered κB sites in the Cxcl1 promoter and enhancer and TF-cofactors facilitate transcription

We next tested how clustered weak κB sites and TF-CoFs support NF-κB binding to DNA, using the regulatory region Cxcl1 gene as a model. We looked for the presence of clustered κB sites within the 500 bp region described in Figure 1A. A 150 bp segment contained at least five κB sites including the strong and a weak site tested earlier with the strong κB site located 57 bp upstream of TSS. In addition to this promoter of Cxcl1, RelA ChIP revealed its binding to a region approximately 15 kb upstream of the Cxcl1 TSS. We assumed that this segment of DNA might be an enhancer of Cxcl1 (**Supplementary Figure 6A**). This segment also contains four weak κB sites and a strong site (GGGATTTCCC; Z-score 8.0) within a ~150 bp segment **(Supplementary Figure 6A**).

To determine if these weak κB sites in the promoter and putative enhancer of the Cxcl1 gene are functional, we used the luciferase reporter assay on wild type (WT) and several mutant constructs, as depicted in **Figure 6A** where the enhancer (E) and the promoter (P) were placed with 0.7 kb spacing. The WT construct, designated as E^{WT}-P^{WT}-TSS exhibited ~20-30-fold higher reporter activity compared to the construct where all κB site were mutated (E^{MT}-P^{MT}-TSS) (**Figure 6B**). The removal of all putative κB sites only within the enhancer (E^{MT}-P^{WT}-TSS) reduced expression by 70%, whereas the removal of all κB sites within the promoter (E^{WT}-P^{MT}-TSS) reduced reporter expression by 90%. We also tested the effect of a DNA fragment that contains a single strong κB site in the promoter (E^{MT}-P^{SSS}-TSS) and a single strong site both in the promoter and enhancer (E^{SSS}-P^{SSS}-TSS). The single strong site in the

promoter (E^{MT}-P^{SSS}-TSS) resulted only in a 2-fold luciferase activity, whereas strong sites both in the enhancer and promoter (E^{SSS}-P^{SSS}-TSS) led to a 3.5x increase, which is about 10% of the activity of the E^{WT}-P^{WT}-TSS DNA. These results suggest that the distal RelA binding region is likely an enhancer and that the weak κB sites potentiate gene activation by efficiently recruiting RelA (**Figure 6B**).

To verify the role of TF-cofactors in transcription activation, we verified reporter expression in the presence of each of the five TF-cofactor by overexpressing them. Overexpression of Cux1 exhibited dramatic induction of reporter expression. Overexpression of Nfat5 also showed higher reporter expression. However, Nfatc1, Smad4 and Tead3 showed no effect in reporter expression (**Figure 6C**). RelA ChIP score in control and TF-cofactor KD HeLa cells showed reduction of ChIP score in all but one (Tead3) compared to the control. It is possible that we used truncated Cux1 and Nfatc1 constructs which possibly act as a potent activator or repressor, respectively, due to the removal of specific domains. Collectively, these results support the notion that specific TF-cofactors act on specific enhancer/promoter.

TF-cofactors and clustered κB sites are essential to form transcriptional condensates

Visualization of transcriptional complex formation, both in vitro and in vivo, has provided important insights into the roles of various factors in the assembly process (Cho et al., 2018; Hnisz et al., 2017; Sabari et al., 2018; Shrinivas et al., 2019). We performed phase-separated condensate formation assays in vitro to assess the role of weak κB sites and TF-CoFs in the assembly of transcription complexes mediated by RelA at the transcription site. We PCR amplified the DNA fragment encompassing the enhancer, promoter and transcription start sites (E^{WT}-P^{WT}-TSS) as present in the luciferase reporter constructs with a Cy3 labeled primer, generating ~1200 bp labeled fragments. Additionally, we amplified mutant DNA with all κB sites mutated (E^{MT}-P^{MT}-TSS) and DNA containing only the strong enhancer and promoter κB sites (E^{SSS}-P^{SSS}-TSS) (**Figure 6A**). Recombinant GFP-$RelA^{FL}$ was mixed with HeLa nuclear extract to monitor condensate formation with Cy3-DNA. We verified that GFP-$RelA^{FL}$ binds DNA, albeit weakly compared to wild-type RelA (**Supplementary Figure 7A**), and found that as high as 2 μM purified recombinant RelA-GFP failed to condense in the absence or presence of DNA under the buffer condition used (150 mM NaCl, 25 mM Tris-HCl 7.5, 100 ng/μL sonicated salmon sperm DNA, 1 mM DTT, 100 ng/μL sonicated salmon sperm DNA, and 2.5 mM $MgCl_2$) (**Figure 7A** & **Supplementary Figure 7B**). However, 100 nM RelA-GFP condensed with DNA (30 nM) in the presence of 1.0 mg/mL TNFa activated HeLa nuclear extract (NE) in this buffer. The reaction mixture was imaged for 20 min with 30 sec image intervals. We looked at the condensates both along the z-axis at the middle of the drop and at the bottom on the cover slip. We noted fewer condensates in the middle of the drop above the cover slip in all cases compared to those on the cover clip (**Supplementary Figures 7C and 7D)**. It is likely that condensates form throughout the drop but settle on the cover slip. In both cases, however, we observed increasing condensate intensity over time and found DNA (red) and RelA-GFP (green) were merged in >90% of these condensates (**Figure 7A and Supplementary 7C**). A few condensates were found in control (E^{MT}-P^{MT}-TSS) and the number was enhanced in E^{SSS}-P^{SSS}-TSS DNA. Qualitative estimation of condensate abundance at 20 or 12

min showed that significantly higher number of condensates were formed with the WT DNA (E^{WT}-P^{WT}-TSS DNA) than with the mutant DNAs (E^{MT}-P^{MT}-TSS and E^{SSS}-P^{SSS}-TSS) (**Figure 7B and Supplementary Figure 7D**). These results indicate that weak κB sites are crucial for recruiting RelA to the enhancer-promoter-TSS DNA, forming the transcription complex. We further verified if DNA condensates from the nuclear extracts containing endogenously activated RelA in the absence of exogenously added RelA-GFP. Indeed, E^{WT}-P^{WT}-TSS DNA, but not E^{MT}-P^{MT}-TSS DNA, formed condensates (**Supplementary Figure 7E**).

We determined RelA-GFP concentration in condensates relative to its concentration in the bulk based on the fluorescence intensity. From a standard curve of increasing concentrations of pure RelA-GFP, the concentration of RelA-GFP in the condensate was estimated to be around 450 nM which is 4.5-fold over the bulk concentration of 100 nM (**Supplementary Figure 7F**). It should be noted that the concentration of unlabeled endogenous RelA is also enhanced. The combined concentration of RelA could be as high as 1 μM in the condensates. This modest enhancement of RelA concentration in the condensates likely results in RelA binding to most κB sites at greater occupancy. Altogether, these findings strongly suggest that cofactors and clustered κB sites in enhancers and promoters cooperate to recruit RelA to the transcription sites of target genes by enhancing RelA's concentrations as depicted in **Figure 6D**.

We further investigated the formation and dynamism of stimulus-induced nuclear RelA condensates in live primary MEF cells expressing mVenus-RelA fusion protein. These cells are derived from the mVenus-RelA reporter mouse (*Rela*$^{V/V}$) in which an mVenus-RelA fusion is knocked in to the endogenous *Rela* locus (Adelaja et al., 2021; Cheng et al., 2021). These cells were treated with LPS for 1 hr followed by imaging (**Figure 7C**). We found nuclear puncta only after stimulation (**Figure 7C**). We performed FRAP (fluorescence recovery after photobleaching) experiments to determine the residence time of RelA in these puncta in MEFs treated with LPS for 1 hr followed by bleaching a cluster of puncta, followed by measuring the recovery rate by collecting images at 0.2 s intervals (**Figure 7D and 7E**). As control, we monitored fluorescence change of another spot that was not bleached (**Figure 7F**). We found the residence time to be ~3.6 s (**Figure 7D and 7E**), which is close to the values determined previously where RelA was overexpressed and two different methods, FRAP and single molecule tracking (SRT) (Bosisio et al., 2006; Callegari et al., 2019). A host of other TF was also investigated for their residence time, and the values were mostly found to be ~10 s (Lu and Lionnet, 2021). These observations suggest that RelA forms dynamic transcriptional condensates likely at the transcription sites in cells. The mechanisms of the dynamic RelA assembly remain to be determined.

DISCUSSION

The functional significance of weak DNA binding sites of TFs has been recognized, primarily through studies on the regulation of developmental genes in vertebrate animals. However, the role of these weak sites in non-developmental programs and how they participate in forming functional transcription complexes remains unclear. Our experiments reveal that weak κB sites, even those showing very little

or no binding in vitro at 1.5 μM RelA concentration, are crucial for recruiting NF-κB RelA to transcription sites and activating transcription in cells. These weak sites help facilitate the assembly of the NF-κB RelA onto the enhancer-promoter-TSS DNA in vitro, and their removal significantly impairs this process. These results imply that clustered κB sites, weak and strong, work together to recruit RelA onto DNA. Previous studies using purified systems demonstrated that tandem κB sites do not facilitate cooperative RelA binding in vitro. This points to the conclusion that cooperative assembly is not accomplished through direct protein-protein contacts between two RelA dimers or indirectly through DNA, pointing towards alternative mechanisms underlying this cooperativity.

We found that recruiting NF-κB RelA dimers to native promoters with clustered κB sites requires numerous cofactors, including TF-cofactors. In this study, we examined five TF-cofactors and observed that their interactions with RelA were weak and that a subset of these TF-cofactors works together with the κB sites in their native context to recruit RelA at specific transcription sites. Each cofactor may interact with multiple RelA dimers using their different domains, thereby facilitating RelA's binding to multiple κB sites. These cofactors may also interact with each other, forming a network of protein-protein contacts guiding RelA to bound to a subset of κB sites within the enhancer/promoter of a target gene. Variations in RelA conformation, dictated by the κB sequences, possibly couple to specific sets of cofactors to drive this process. Notably, these TF-cofactors appear to function without requiring their own DNA binding, as no enrichment of binding sites was observed for at least two of the TF-factors tested (Cux1 and Smad4). Although we cannot entirely rule out the possibility that other cofactors, Nfatc1, Nfat5 and Tead3, bind to DNA since their binding sites overlap κB sites. However, this sequence overlap suggests that direct DNA contact by these cofactors would reduce NF-κB RelA recruitment. Our observations also align with numerous reports demonstrating that TFs can be recruited to DNA without binding directly to cognate DNA sites (Gordan et al., 2009).

We argue that activated nuclear RelA is trapped by these cofactors at DNA, significantly enhancing RelA concentrations, enabling RelA to bind these weak sites efficiently. In addition to TF-cofactors, we identified other classes of cofactors. It is not clear if all these cofactors facilitate RelA recruitment to DNA like the TF-cofactors or if some of these cofactors perform other functions on RelA such as its modifications. The presence of RBPs and different enzymes as RelA cofactors entices us to propose a new model of transcription complex assembly on DNA. The RNA binding protein may simultaneously bind both RelA and ncRNAs, stabilizing the assembly complexes (Scott et al., 2024; Xiao et al., 2019). It is also likely that RelA simultaneously binds ncRNA, as reported in other cases (Hudson and Ortlund, 2014; Oksuz et al., 2023). Enzymes such as kinases, methylases, acetylases, deacetylases and glycosylases might be involved in protein and DNA modifications and demodifications. Such modification processes could explain the transient nature of the RelA:DNA complex as observed here and reported previously (Bosisio *et al.*, 2006; Callegari *et al.*, 2019). In a specific modified state, the complex dissociates slowly, whereas in another state, dissociation is fast. We propose that transient binding is mediated by modifications and not by mass-action driven binding kinetics as generally considered to understand DNA binding (Brignall et al., 2019; Oksuz *et al.*, 2023). Given that RelA concentrations are significantly amplified in the condensates in vitro, RelA

concentrations in the condensates in vivo are expected to be high. We suggest that without the action of modifying enzymes, most κB sites would remain bound to RelA with long half-lives, as observed in vitro (Li et al., 2024).

It is not entirely clear how the κB sites in a cluster function. It is possible that during transcription, only a subset of κB sites within the cluster is active at any given time, assembling RelA with the support of cofactors. This subset may rapidly switch to a different subset at another time. Rather than forming a single transcription complex centered around a strong site, multiple complexes may form dynamically utilizing different combinations of κB sites and cofactors. If all κB sites would be equally important and acted simultaneously and cooperatively, we would expect more pronounced defects upon deletion of each κB site. Instead, we found that the deletion of any one of the three weak κB sites in Nfkbid only partially reduced RelA binding and transcription. These complexes are cooperative and specific but not stable, as each κB site within the clusters exhibits partial independence in DNA and cofactor binding. This independence allows single bp changes to alter activity, contributing to a flexible, malleable complex that is finely regulated by both protein and DNA modifications (Leung et al., 2004; Wang et al., 2012).

In conclusion, our results indicate that cognate κB DNA binding by NF-κB RelA is significantly more complex than can be explained simply by direct contacts between the protein and DNA. Although transcription was found to be synergistic in cells, cooperative interactions between two NF-kB dimers bound to tandem sites were observed in vitro. Our findings highlight a multilayered assembly involving multiple κB sites, numerous cofactors, and NF-κB RelA itself. This assembly enhances NF-κB concentration at DNA, allowing it to bind weak sites. We propose that multiple RelA dimers, along with other TFs that do not directly contact DNA, use their activation domains to recruit mediator complexes and RNA polymerase II, facilitating transcription.

Materials and Methods

Antibodies and Reagents

The RelA (8242), H3 (9715), HDAC3 (3949) and p50 (13586) antibodies used in Western Blots and EMSA supershifts were purchased from Cell Signaling Technology. The IκBα (0040) and tubulin (0119) antibodies were purchased from BioBharati LifeScience. The FLAG (F1804) antibody was purchased from Sigma-Aldrich. The Nfatc1 (7294) antibody was purchased from Santa Cruz Biotechnology. The RelA antibody (C15310256) used for ChIP-Seq was purchased from Diagenode. Mouse TNFα (BioBharati) was used at a final concentration of 10 ng/mL for the indicated timepoints.

Mammalian Cell Culture and Generation of Stable Cell Lines

WT MEF, RelA-KO MEF, mVenus-tagged RelA MEF, HeLa, and 293T cells were cultured in Dulbecco's modified Eagle's medium (Corning) supplemented with 10% FBS (Corning) and antibiotics.

For generation of stable CRISPR-modified MEF cell lines, gRNA targeting a 20 nt genomic region adjacent to a Cas9 protospacer adjacent motif (PAM) was first annealed and cloned into BsmbI (NEB) digested pLentiCRISPRv2 vector. Sanger sequencing was performed verify cloning. The different pLentiCRISPRv2 gRNA constructs were then cotransfected with pMDLg/pRRE, pCMV-VSV-G, and pRSV-Rev expression constructs into HEK293T using TransIT-Lenti transfection reagent (Mirus) for generation of lentiviral particles. After 24 hours, viral supernatant was harvested and filtered through a 0.4 µm filter and used to infect MEF at a dilution of 1:10 in the presence of 10 ng/µL polybrene (MilliporeSigma) for 48 hours. MEF was then selected and grown in media containing 5 µg/mL puromycin. Generation of stable shRNA knockdown MEF cells was carried out similarly, with the exception that annealed oligoes for shRNA targets were cloned into the pLKO.1 TRC vector digested with AgeI and EcoRI, which was then cotransfected in HEK293T for generation of viral particles.

Protein Expression and Purification

Full length His-RelA and His-GFP-RelA (1-551) were expressed in *Spodoptera frugiperda* Sf9 insect cells using the Bac-to-Bac baculoviral expression system as previously described. Briefly, baculovirus infected Sf9 cells were sonicated in lysis buffer containing 25 mM Tris-HCl pH 7.5, 500 mM NaCl, 5% glycerol, 0.1% NP-40, 20 mM imidazole, 5 mM β-mercaptoethanol, and 0.5 mM PMSF. The lysate was clarified by centrifugation and incubated with Ni-NTA agarose beads (BioBharati). Beads were extensively washed with lysis buffer without PMSF and bound RelA was eluted with lysis buffer containing 250mM imidazole and no PMSF. Elutions were pooled, concentrated, and separated on a HiLoad 16/60 Superdex 200 (Cytiva) size-exclusion column with buffer containing 25 mM Tris-HCl pH 7.5, 200 mM NaCl, 5% glycerol, and 1 mM DTT. Peak fractions were pooled, concentrated, and flash frozen in liquid nitrogen.

For preparation of recombinant p50:RelA heterodimer, first His-tagged p50 (1-435) was transformed into *E. coli* Rosetta (DE3). Isolated colonies were used to inoculate a 2 L LB culture, which was grown to an OD_{600} of 0.2 at 37 °C and induced with 0.25 mM isopropyl β-D-thiogalactpyranoside (IPTG) for 18 h at 25 °C. Cells were harvested by centrifugation and sonicated in lysis buffer containing 25 mM Tris-HCl pH 7.5, 250 mM NaCl, 10% glycerol, 0.1% NP-40, 10 mM imidazole, 0.25 mM PMSF, and 5 mM β-mercaptoethanol. Lysate was clarified by centrifugation and incubated with Ni-NTA agarose beads (BioBharati). Beads were washed with lysis buffer
and recombinant His-tagged p50 was eluted from Nickel-NTA agarose beads in the same buffer except with 250 mM imidazole. The purified p50 was concentrated and incubated in a 1:1 molar ratio with His-tagged RelA (1- 551) at a final concentration of 0.1 mg/mL in buffer containing 25 mM Tris-HCl pH 7.5, 250 mM NaCl, 10% glycerol, and 1 mM DTT for 1 hour at room temperature. The p50:RelA heterodimer was then concentrated and separated on a HiLoad 16/60 Superdex 200 size-exclusion column with buffer containing 200 mM NaCl, 25 mM Tris-HCl, 5% glycerol and 1 mM DTT. Peak fractions were collected, concentrated, and flash frozen in liquid nitrogen.

Crystallization of κB DNAs and RelA:κB complexes

For crystallization of RelA:κB-DNA complexes, κB-DNA duplexes were first generated as described before. Complexes were formed by incubating untagged RelA(19-304) at a final concentration of ~150 micromolar with κB-DNAs in 1:1.2 molar ratio in buffer containing 25 mM Tris-HCl pH 7.5, 50mM NaCl, and 1mM DTT for 15 minutes at room temperature. Crystals were obtained using hanging drop vapor diffusion method by mixing complexes with reservoir solution containing MES pH 5.5, 2 mM calcium chloride, 50 mM ammonium chloride, 14 % PEG3350, 1 mM spermine, and 0.05 % octyl β-D-glucopyranoside in a 1:1 ratio at 18 °C. Crystals nucleated around the fourth day and reached a maximum size around the 10th day. Crystals were soaked in the mother liquor without DTT containing 21 % ethylene glycol for cryo-protection, and flash frozen in liquid nitrogen.

RelA Promoter Analysis

Using previously published RelA ChIP-Seq data sets in TNFα stimulated MEF, RelA motifs at RelA ChIP-Seq peaks were identified using the JASPAR database. RelA binding at JASPAR-identified motifs were then quantified and sorted based on ChIP-Seq intensity at the strongest local motif. The genomic region encompassing the flanking +/- 500 bp around the motif of each peak was then analyzed for the presence of additional low-affinity RelA motifs utilizing sequences and Z-scores from previous p50:RelA SELEX data. A Z-score cutoff of 6 was used binarize strong versus weak binding sites for counting of motifs based on previous *in vitro* studies of known weak motifs. Pearson correlation analysis was performed by analyzing the cumulative Z-score upon adjusting the window surrounding the RelA motif from a range of 10 to 500 bp.

RNA-Seq and RNA-Seq Analysis

RNA-seq was performed in experimental triplicates as previously described. 5 million knockdown and control cells were plated in 6-well plates the day before stimulation. Cells were stimulated with 10 ng/mL TNFα for 1 hour, washed once with PBS, and RNA was isolated using TRIzol (Invitrogen) following manufacturers recommendation. RNA was quantified by nanodrop, and integrity was measured with Tapestation (Agilent) before proceeding with library preparation. DNA libraries were prepared from 1 ug of total RNA using KAPA mRNA Hyperprep Kit (Roche) with KAPA Unique Dual-Indexed adapters (Roche). Libraries underwent 8 cycles of PCR amplification and were analyzed by Tapestation (Agilent). Libraries were then quantified by dsDNA Qubit (Thermo), pooled, and underwent 100 bases of paired-end sequencing using the NovaSeq 6000 S4 sequencer (Illumina).

Sequencing quality was first assessed by FastQC and libraries with high quality reads were trimmed using Trimmomatic (v0.39). Reads were then mapped to the mm10 mouse reference genome using STAR (v2.7.10b) and transcripts were quantified using StringTie (v1.3.6). Counts were imported to R using prep.de.py3 for normalization and differential expression analysis with DESeq2 (v1.42.0).

ChIP-Seq and ChIP-Seq Analysis

Chromatin immunoprecipitation (ChIP) was performed in two biological duplicates as previously described. Following 30 min stimulation with 10 ng/mL TNFα, knockdown and control MEF cell lines

were washed once with PBS then crosslinked with 2 mM disuccinimidyl glutarate (DSG) (ProteoChem) in PBS for 30 min at room temperature with gentle rocking, followed by a second crosslinking with 1% (vol/vol) formaldehyde in PBS for 10 min at room temperature. Crosslinking was quenched upon the addition of 125 mM glycine and room temperature incubation for 5 min. Cells were washed twice with ice-cold PBS and harvested by scraping. Nuclear fractionation was performed with gentle resuspension of the cellular pellet in 1 mL of PBS supplemented with 0.5% NP-40 and 0.5 mM PMSF, followed by rotation at 4 °C for 10 min. The nuclear pellet was collected by centrifugation, washed once with PBS containing 0.5 % NP-40, then washed with PBS, followed by resuspension in 1 mL RIPA buffer (25 mM Tris-HCl pH 7.5, 150 mM NaCl, 0.1% SDS, 0.1% sodium deoxycholate, 1% NP-40, 1 mM EDTA, 1 mM DTT, and 0.5 mM PMSF). Chromatin was sonicated to an approximate size distribution of 200-1000 bp using a Model 120 sonic dismembrator (Fisher) with 2 mm diameter tip with the following settings:15 total cycles, 20 second pulse intervals with 40 seconds dwell time, and 80% amplitude. Samples were then centrifuged at 13,000 g for 10 min at 4 °C. Supernatant containing sonicated chromatin was then diluted 1:1 with dilution buffer containing 25 mM Tris HCl pH 7.5, 150 mM NaCl, 1 mM EDTA, 1 mM DTT, and 0.5 mM PMSF before use in immunoprecipitation. For each immunoprecipitation, 30 µL of Protein G Magnetic beads (NEB) was mixed with 1 µL of anti-RelA antibody (Diagenode) in PBS containing 0.5% (m/v) BSA. Beads were then washed three times with PBS before final resuspension in binding buffer containing 25 mM Tris-HCl pH 7.5, 150 mM NaCl, 0.05% SDS, 0.05% sodium deoxycholate, 0.5% NP-40, 1 mM EDTA, and 1 mM DTT. Beads were then mixed with sonicated chromatin and incubated overnight at 4 °C with rotation. Beads then underwent the following wash steps with 2 min rotation at room temperature between each step unless otherwise specified: 3 washes with binding buffer, 3 washes in buffer containing 10 mM Tris-HCl pH 7.5, 250 mM LiCl, 1% NP-40, 0.7% sodium deoxcholate, and 1 mM EDTA, 2 washes for 30 min in buffer containing 10 mM Tris-HCl pH 8.0, 1 mM EDTA, and 0.2% Tween 20, and 2 washes in buffer containing 10 mM Tris-HCl pH 8.0, 0.1 mM EDTA, and 0.05% Tween 20. Beads were then resuspended in 25 µL of buffer contain 10 mM Tris-HCl pH 8.0 and 0.05% Tween 20. Libraries were then prepared on beads using NEBNext Ultra II DNA Library Prep kit (NEB) following manufacturers recommendations with 0.6 µM of KAPA Unique Dual-Indexed adapters (Roche). To each 46.5 µL reactions, 16 µL of nuclease free water, 4 µL of 10% SDS, 4.5 µL of 5 M NaCl, 3 µL of 0.5 M EDTA, 4 µL of 0.2 M EGTA, 1 µL of 20 mg/mL Proteinase K (NEB), and 1 µL of 10 mg/mL RNase A (Qiagen) was added. The reaction was incubated at 55 °C for 1 hour for Proteinase K and RNase A digestion, followed by 65 °C incubation overnight to reverse-crosslinking. DNA was purified with 50 µL of Ampure XP beads (Beckman Coulter) and 20% PEG8000/2.5 M NaCl at a final concentration of 12% PEG and eluted in 13 µL 10 mM Tris-HCl pH 8.0 and 0.05% Tween 20. The eluted DNA was PCR amplified with KAPA HiFi 2x HotStart ReadyMix (Roche) and 10x Library Amplification Ready Mix primers (Roche) for 16 cycles. PCR amplified libraries were then purified with Ampure XP beads at a 1:1 ratio (10% PEG final), analyzed by TapeStation (Agilent), and quantified by dsDNA Qubit (Thermo) before pooling. Pooled libraries were then size selected with Pippin HT (Sage Science) to a size range of 200-500 bp and 50 bp paired-end sequenced on the NovaSeq X Plus (Illumina).

ChIP-Seq analysis was performed as previously described (Abe et al., 2023). Sequencing quality was first assessed by FastQC and libraries with high quality reads were trimmed with Trimmomatic (v0.39). Trimmed FASTQ files were then mapped to the mm10 mouse reference genome using Bowtie2. Peaks were then called using HOMER (findPeaks) with the parameters "-style factor -L 0 -C 0 -fdr 0.9 -minDist 200 -size 200 -o auto". Raw tag counts were quantified with HOMER (annotatepeaks.pl) and tag counts were averaged between experimental replicates.

Luciferase Assays

Complementary primers of specific promoters were first annealed by mixing at a final concentration of 2μM in buffer containing 10 mM Tris-HCl pH 7.5, 50 mM NaCl, and 1 mM EDTA and incubating in boiling water allowed to slowly cool to room temperature. Annealed promoters were then cloned into the CMXTK-Luciferase vector (a kind gift from Dr. Chakravarti at Northwestern University Feinberg School of Medicine) at the SalI and BamHI restriction sites. HEK293T were grown in 12-well plates and transiently transfected using PEI with HA-RelA (1- 551) or control empty HA-vector, the luciferase reporter DNAs, and control CMV-driven Renilla. Cells were collected 24 h post-transfection and lysate was collected and used for luciferase activity assay using the Dual-Luciferase Reporter Assay System (Promega). Data are represented as mean ± standard deviations (SD) of three or more independent experimental replicates.

Elecrophoretic Mobility Shift Assays

Oligonucleotides were ^{32}P end radiolabeled using T4-polynucleotide kinase (New England Biolabs) and [γ-^{32}P]ATP (PerkinElmer), purified from free [γ-^{32}P]ATP using a Microspin G-25 column (Cytiva), and annealed with complementary DNA. Recombinant RelA or p50:RelA were incubated with radiolabeled DNA at room temperature for 15 minutes in binding buffer containing 10 mM Tris- HCl pH 7.5, 50 mM NaCl, 10% glycerol, 1% NP-40, 1 mM EDTA, and 0.1 mg/mL sonicated salmon sperm DNA (Fisher). Proteins were diluted in dilution buffer containing 20 mM Tris-HCl pH 7.5, 50 mM NaCl, 10% glycerol, 1 mM DTT, and 0.2 mg/mL bovine serum albumin in preparation for the reaction mixture. Complexes were analyzed by electrophoresis in a pre-ran 5% non-denatured polyacrylamide gel at 200 V for 1 h at room temperature in 25 mM Tris, 190 mM glycine, and 1 mM EDTA. Gel was then dried, exposed on a phosphor screen overnight, and scanned by Typhoon FLA 9000 imager (Cytiva).

For EMSA with 293T nuclear extract, cells were first transfected with either empty vector or HA-tagged full-length RelA overexpression plasmid using TransIT-Lenti (Mirus) following the manufacturers recommendations. 24 hours after transfection, cells were harvested by scraping in PBS and lysed in cytoplasmic lysis buffer consisting of PBS with 0.1% NP-40 and 0.5 mM PMSF. Nuclei were then pelleted by centrifugation at 300 g, washed twice with PBS, and resuspended in nuclear extraction buffer consisting of 25 mM Tris-HCl pH 7.5, 420 mM NaCl, 10% glycerol, 0.2 mM EDTA, 1 mM DTT, and 0.5 mM PMSF. Nuclear extract was quantified by Bradford assay and 7 μg of extract was mixed with radiolabeled DNA in a binding reaction consisting of 25 mM Tris-HCl pH 7.5, 150 mM

NaCl, 10% glycerol, 1 mM EDTA, and 0.1 mg/mL sonicated salmon sperm DNA. Complexes were analyzed by non-denaturing gel electrophoreses as outlined previously.

RNA Isolation and Real-Time qPCR

Total RNA was isolated from cultured cells by isopropanol precipitation with TRIzol (Invitrogen) following manufacturers recommendations. RNA concentration was determined by nanodrop, and 1 µg of total RNA was used for cDNA synthesis using Maxima H Minus Master Mix (Thermo Scientific) in a reaction volume of 5 µL. Synthesized cDNA was then diluted 4- fold and 1 µL was used as template for real-time qPCR using Luna Master Mix (NEB). Values were normalized to GAPDH, and data was represented at mean ± standard deviation (SD) from three independent experimental replicates.

***In vitro* Pulldown Assays, Mass Spectrometry, and Analysis**

For FLAG pulldown assays in HEK93T, cells were transfected with empty vector or FLAG-Nfatc1, Nfat5, Tead3, Cux1, or Smad4 overexpression constructs using PEI. After 24 hours, cells were stimulated with mouse TNFα for 30 minutes, washed once with ice-cold PBS, and lysed in lysis buffer containing 25 mM Tris-HCl pH 7.5, 150 mM NaCl, 5% glycerol, 1% NP-40, 1 mM DTT, and 0.25 mM PMSF. Lysate was clarified by centrifugation and incubated for 2 hours at 4 °C with anti-FLAG M2 agarose beads (Sigma) with gentle rotation. Beads were extensively washed with lysis buffer before adding 4x SDS gel loading dye to a final concentration of 1x. Beads were incubated on a 95°C heat block for 5 minutes and loaded on gel for Western blot analysis.

For streptavidin-DNA pulldown assays, 5' biotinylated oligonucleotides (IDT) were annealed with corresponding nonbiotinylated reverse complement oligonucleotides at a final concentration of 45 µM as previously outlined. For each pulldown reaction, 40 µL of 45 µM annealed DNA was mixed with 100 µL of Neutravidin agarose resin (Thermo) at a total volume of 400 µL in buffer containing 10 mM Tris-HCl pH 7.5, 50 mM NaCl, and 0.5 mM EDTA. Biotinylated DNA was immobilized onto beads by incubation for 1 hour at room temperature with gentle rotation. Beads were then washed extensively with pulldown buffer containing 25 mM Tris-HCl pH 7.5, 150 mM NaCl, 5% glycerol, 0.1% NP-40, and 1 mM DTT with final resuspension in 50 µL per pulldown. MEF nuclear extract was prepared following 30 minutes of 20 ng/mL mouse TNFα treatment as previously outlined. Approximately 250 µg of nuclear extract was diluted 2.8-fold with pulldown buffer without NaCl but supplemented with 0.5 mM PMSF to reduce the final NaCl concentration from 420 mM to 150 mM. The diluted extract was then mixed with the double mutant M5 beads and precleared by gentle rotation at 4°C for 2 hours. Mutant beads were then pelleted and discarded, and the precleared lysate was mixed with the corresponding experimental beads overnight at 4 °C with gentle rotation. For Western analysis, beads were extensively washed and resuspended in 4x SDS gel loading dye to a final concentration of 1x. Beads were then incubated on a 95 °C heatblock for 5 minutes and analyzed by Western blot. Microcapillary LC/MS/MS for peptide identification was conducted at the Taplin Biological Mass Spectrometry Facility at Harvard Medical School using Orbitrap mass spectrometers (Thermo).

For analysis of MEF mass spectrometry data, values corresponding to total peptides identified were used. Identified peptides were filtered to exclude peptides containing less than 5 total across all experiments. Total peptides were then normalized by dividing by sum total of peptides across all samples. Normalized peptides were then Z-score converted and further filtered to include peptides enriched in pulldown for biotin-Cxcl2 DNA or biotin-Ccl2 DNA over biotin-control DNA.

Biolayer Interferometry Assay and Analysis

We adopted the method as desctibed by Li et al (Li *et al.*, 2024). Briefly, biotinylated oligonucleotides were annealed with complementary nonbiotinylated oligonucleotides by mixing at a ratio of 1:1.2 in buffer containing 10 mM Tris-HCl pH 7.5, 50 mM NaCl, and 1 mM EDTA and incubating in boiling water allowed to slowly cool to room temperature. Biotinylated annealed DNA (200 nM) was then immobilized onto hydrated Octet Streptavidin (SA) biosensors (Sartorius) for 10 seconds in BLI buffer consisting of 25 mM Tris-HCl pH 7.5, 150 mM NaCl, 0.02% Tween 20, 0.1 mg/mL sonicated salmon sperm DNA, and 1 mM DTT using the Octet K2 system (ForteBio). A reference sensor without DNA was used for background subtraction. Baseline was first measured by incubation of sensors in BLI buffer for 60 seconds. Binding kinetics were then measured through an association phase of 120 seconds in which 12.5, 25, 50, 100, or 200 nM of recombinant His-RelA (1-551) was incubated with the biotinylated DNA-sensor complex, followed by a dissociation phase of 180 seconds in BLI buffer without protein. Sensor was regenerated in BLI buffer containing 1 M NaCl for 5 seconds followed by wash in BLI buffer for another 5 seconds three times prior to each reading.

Nuclear RelA Concentration Assay

A confluent 10 cm plate of HeLa cells to be used as a reference for cell number was collected by trypsinization and counted using a hemacytometer. Cells were then pelleted by centrifugation at 4,000 rpm for 2 min at 4 °C. Cell pellet was washed once with PBS, followed by lysis in RIPA buffer containing 25 mM Tris-HCl pH 7.5, 150 mM NaCl, 0.1% SDS, 0.1% sodium deoxycholate, 1% NP-40, 1 mM EDTA, 1 mM DTT, and 0.5 mM PMSF. Lysate was centrifuged at 13,000 rpm for 15 min at 4 °C and supernatant was collected. Additional confluent plates of HeLa cells were stimulated with 10 ng/mL TNFα or control DMSO for 30 min. Cells were then washed and collected in ice cold PBS by scraping. Cells were pelleted by centrifugation at 4,000 rpm for 2 minutes at 4 °C and resuspended in cytoplasmic lysis buffer containing PBS with 0.05% NP-40 and 0.5 mM PMSF. The resuspended cells were incubated for 10 min at 4 °C with rotation. Crude nuclei were harvested by centrifugation at 4,000 rpm for 2 minutes at 4 °C and the supernatant was collected as the cytoplasmic fraction. Crude nuclei were then resuspended in buffer containing PBS with 0.2% NP-40 and 0.5 mM PMSF and rotated for 10 min at 4 °C. Nuclei were harvested by centrifugation at 6,000 rpm for 2 minutes at 4 °C, washed once with PBS, and resuspended in nuclear extraction buffer containing 25 mM Tris-HCl pH 7.5, 420 mM NaCl, 10% glycerol, 0.2 mM EDTA, 1 mM DTT, and 0.5 mM PMSF. Resuspended nuclei were incubated on ice for 15 min and centrifuged at 13,000 rpm for 15 min at 4 °C. Supernatant was collected as nuclear fraction. Immunoblot analysis using anti-RelA antibody of nuclear extract compared to recombinant

full-length RelA was used for RelA quantitation and immunoblot analysis using anti-Lamin B1 of nuclear extract with whole cell lysate standard was used for nuclei quantitation. An average HeLa nuclear volume of 374 μm^3 (Maul and Deaven, 1977) and 1 nuclei per cell were used for calculation of nuclear volume from nuclei count.

In vitro Condensate Formation Assay and Quantification

Cy3-labeled enhancer-promoter DNAs used for condensation assay were generated by PCR using Taq polymerase (NEB) with a Cy3-labeled primer (IDT) and different template constructs. PCR products were analyzed by agarose gel electrophoresis and purified with Monarch PCR and DNA Cleanup Kit (NEB). On a passivated glass coverslip, 4 µL droplets containing 100 nM GFP-RelA, 1 mg/mL TNFα-stimulated HeLa nuclear extract, and 80 ng of Cy3-labeled Cxcl1 enhancer-promoter DNA was prepared in buffer containing 25 mM Tris-HCl pH 7.5, 150 mM NaCl, 1 mM DTT, 0.5 mM $MgCl_2$, and 0.1 mg/mL sonicated salmon sperm DNA. The droplet was mixed by pipetting and 3 µL was removed to leave 1 µL remaining on the coverslip. The droplet was covered with another coverslip separated by a rubber spacer to prevent drying. Droplets were visualized using a Nikon Eclipse Ti2-E widefield fluorescence microscope at 100x magnification and images were captured every minute after 5 min incubation at room temperature for a total acquisition time of 15 min.

For quantitation of GFP-RelA concentration within condensates, a standard curve was generated for background subtracted fluorescence intensity of GFP-RelA at concentrations of 100, 200, 400, 600, 800, and 1000 nM on the same coverslip. Average background subtracted peak fluorescence intensity of 10 condensates was measured and compared with standard curve for concentration calculation.

Live Cell Imaging

Live cell imaging and FRAP experiments were performed at the Nikon Imaging Center at UCSD using a Nikon Ti-2 Eclipse and CSU W1 SORA confocal microscope with FRAP modality. mVenus-tagged RelA mouse embryonic fibroblasts were kindly provided by Dr. Alexander Hoffmann (Adelaja *et al.*, 2021). Cells were plated on glass bottom 35 mm plates (Mattek) the day before live cell imaging. Cells were then treated with either 10 ng/mL TNFα for 30 minutes, 100 ng/mL LPS for 1 hour, or control DMSO before imaging. 15 minutes before imaging, 1 drop of NucRed Live 647 ReadyProbes reagent (Thermo) was added for nuclear staining. For dual color imaging, an excitation of 470/40 nm and emission of 525/50 nm was used for fluorescence detection of mVenus-RelA and an excitation of 620/60 nm and emission of 700/75 nm was used for nuclei detection. For FRAP, concentrated signal of mVenus-RelA was bleached with 405 nm illumination with an exposure time of 200 ms. Signal recovery was quantitated at the region of interest every 0.2 s. A non-photobleached region of identical size was quantified as control. Each frame was background corrected for photobleaching by subtraction against a non-targeted region.

Immunoprecipitation Assay

HEK293T cells were cotransfected on 6-well plates with plasmids containing either empty vector or FLAG-tagged Nfatc1, Nfat5, Tead3, Cux1, or Smad4 with HA-tagged RelA (1-551) using polyethylenimine (PEI). After 24 hours, cells were washed once with PBS and lysed in 200 μL non-denaturing lysis buffer containing 25 mM Tris-HCl pH 7.5, 150 mM NaCl, 5% glycerol, 1% NP-40, 1 mM DTT, and 0.5 mM PMSF. Lysate was clarified by centrifugation at 13,000 rpm for 10 min at 4 °C and incubated with anti-FLAG M2 agarose beads (Sigma) for 2 hours at 4 °C with rotation. Beads were then extensively washed and precipitated proteins were analyzed by SDS-PAGE and Western blot.

ACKNOWLEDGEMENTS The work was supported by NIH grant GM085490 to GG. SS was supported by the CMG training grant during his PhD. Authors thank Dr. Alex Hoffmann of UCLA for providing RelA-Venus MEFs and for helpful discussion. We that Dr. Tom Huxford of San Diego State University for reading and editing the manuscript. The authors also than the NIKON microscopy facility at UCSD for support.

CONFLICT OF INTEREST

GG and TB are cofounders of Siraj Therapeutics. SS is partially supported by Siraj Therapeutics. The authors declare that they have no conflicts of interest with the contents of this article. The content is solely the responsibility of the authors and does not necessarily represent the official views of the National Institutes of Health.

AUTHOR CONTRIBUTIONS

G.G. conceived the original idea. S.S. further refined the idea and conducted most experiments. T.B, Y.S., R.S. and Y.Z. performed experiments. G.G. wrote the original draft which was modified by all S.S. and T.B. All other authors read the manuscript.

Figures and Figure Legend

Figure 1

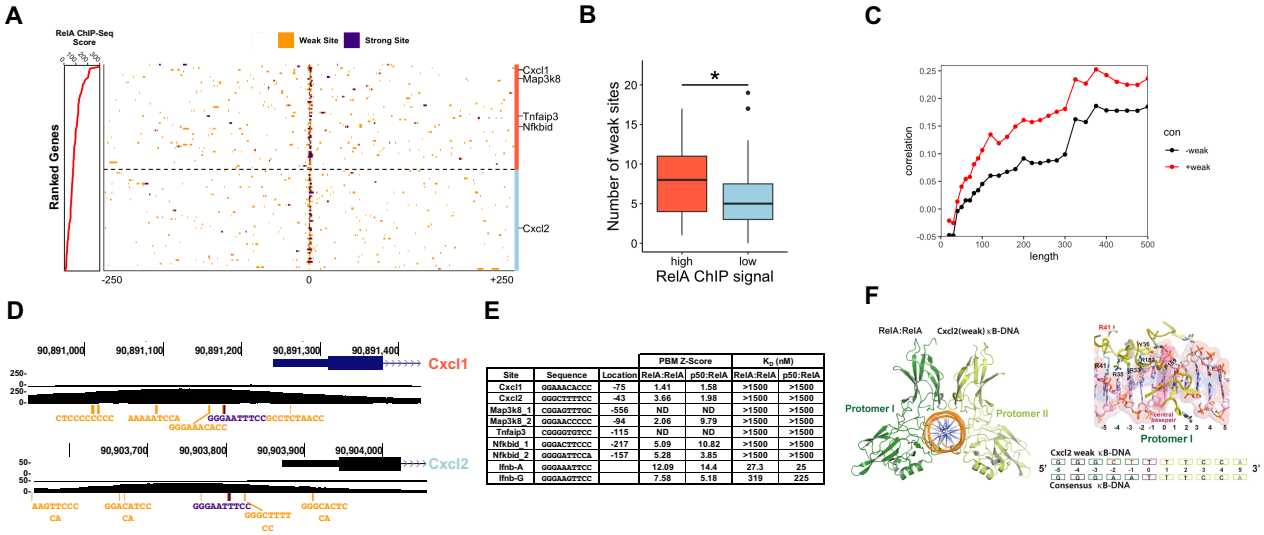

			PBM Z-Score		K_D (nM)	
Site	Sequence	Location	RelA:RelA	p50:RelA	RelA:RelA	p50:RelA
Cxcl1	GGAAACACCC	-75	1.41	1.58	>1500	>1500
Cxcl2	GGGCTTTTCC	-43	3.66	1.98	>1500	>1500
Map3k8_1	CGGAGTTTGC	-556	ND	ND	>1500	>1500
Map3k8_2	GGGAACCCCC	-94	2.06	9.79	>1500	>1500
Tnfaip3	CGGGGTGTCC	-115	ND	ND	>1500	>1500
Nfkbid_1	GGGACTTCCC	-217	5.09	10.82	>1500	>1500
Nfkbid_2	GGGGATTCCA	-157	5.28	3.85	>1500	>1500
Ifnb-A	GGGAAATTCC		12.09	14.4	27.3	25
Ifnb-G	GGGAAGTTCC		7.58	5.18	319	225

Figure 1. Analysis of promoter regions of RelA-regulated genes that are stimulated by TNFa within 30 min.

A. Right, ChIP-seq data (publicly available) were analyzed for the presence of weak and strong κB motifs, as defined by cut-off Z-score of 6 from PBM analysis of p50:RelA heterodimer and RelA homodimer (Siggers, et al. 2009), within a 500 bp window centered around ChIP peak (Kim, et al. 2020). The dotted line demarcates high and low RelA ChIP binding in analyzed promoter regions. Left, the plot of ranked genes versus RelA ChIP score.

B. Plot of RelA ChIP-seq scores versus number of κB sites in the top and bottom half of 100 ranked genes.

C. Comparison of the correlation between RelA ChIP binding and cumulative promoter Z-score with length of window analyzed surrounding central κB site, with correlation peaking around DNA length of around 300 bp.

D. The map of κB sites, their sequences, and RelA ChIP-seq scores in Cxcl1 and Cxcl2 promoters within the 500 bp window of ChIP-seq peak. Strong and weak κB site sequences in purple and orange, respectively. RelA ChIP scores are indicated in left.

E. Equilibrium binding affinity (this study) with Z-scores (Siggers, et al. 2009) of κB sites for RelA homodimer and p50:RelA heterodimer.

F. A cartoon representation of the RelA homodimer (left) bound to a weak κB site (bottom). Structural similarity/dissimilarities in interaction of the RelA protomer to half sites in weak versus strong κB sites (right).

Supplementary Figure 1

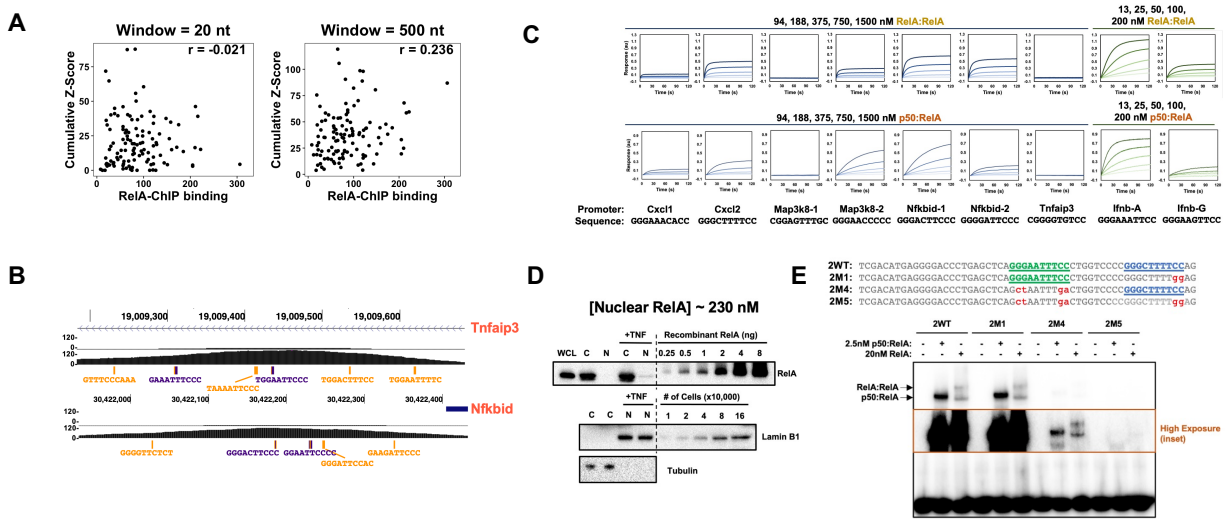

Supplementary Figure 1.

A. The correlation plots between RelA-ChIP score and cumulative Z-score over a 20 bp window around the strong site (left), and a 500 bp window (right).

B. The map of κB sites, their sequences, and RelA ChIP-seq scores in Tnfaip3 and Nfkbid within the 500 bp window of ChIP-seq peak. Strong and weak κB site sequences in purple and orange, respectively.

C. The binding of κB site sequences to full-length RelA homodimer (top) and p50:RelA heterodimer (bottom) by BioLayer interferometry assay. Binding to Ifnb-A and Ifnb-G, present in many promoters, are assessed as control κB sites.

D. Immunoblot analysis of RelA from whole cell lysate (WCL), cytoplasm (C), and nuclear (N) fractions with or without TNFa stimulation. Recombinant purified RelA was used as a standard for quantitation of RelA amount, and Lamin B1 was used for a standard of cell number.

E. The electrophoretic mobility shift assay (EMSA) with wild-type and mutant sequences derived from Cxcl2 gene promoter. The Cxcl2 promoters with mutation (marked in red) of strong and/or weak sites abolishing affinity to RelA. The sequence of strong and weak κB sites are colored green and blue, respectively.

Figure 2

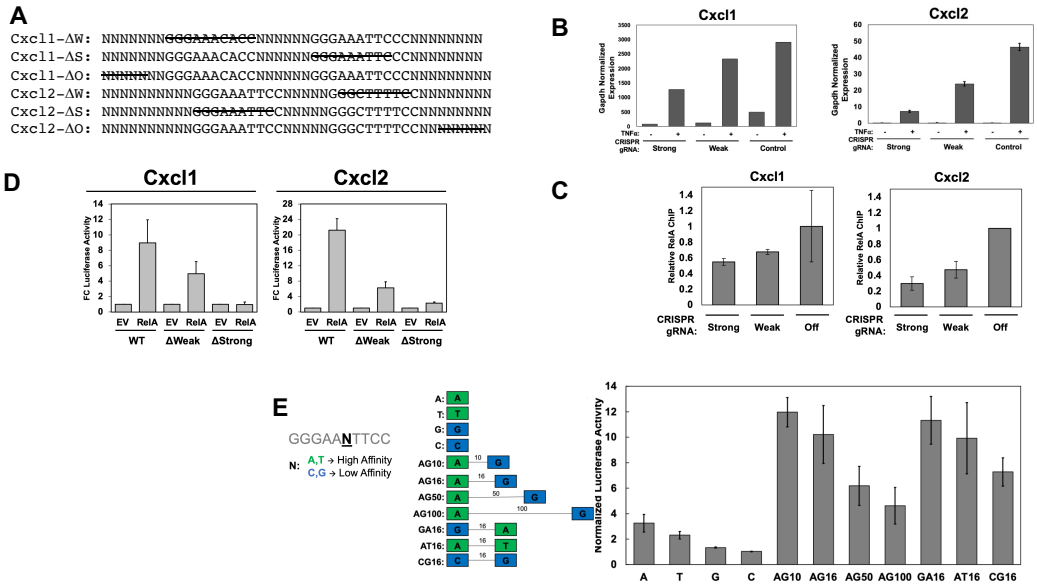

Figure 2. Multiplicity of κB sites (strong and weak) influence recruitment of RelA and transcription.
A. A schematic of the arrangements of strong and weak κB sites (and an off-target random site) of Cxcl1 and Cxcl2 promoter regions for CRISPR deletion.
B. Transcript levels of Cxcl1 and Cxcl2 with their strong, weak, or a random site deleted by CRISPR in MEF cells upon TNFa stimulation at 1 h determined by RT-qPCR.
C. RelA ChIP signals at Cxcl1 and Cxcl2 promoters containing deletion of strong, weak or a non-κB site (control).
D. Luciferase reporter expression from reporter plasmids containing wild-type or mutant Cxcl1 or Cxcl2 promoter regions in HeLa cells transfected with RelA expression vector.
E. Luciferase reporter expression from reporter plasmids under indicated synthetic promoters in HeLa cells transfected with RelA expression vector.

Supplementary Figure 2

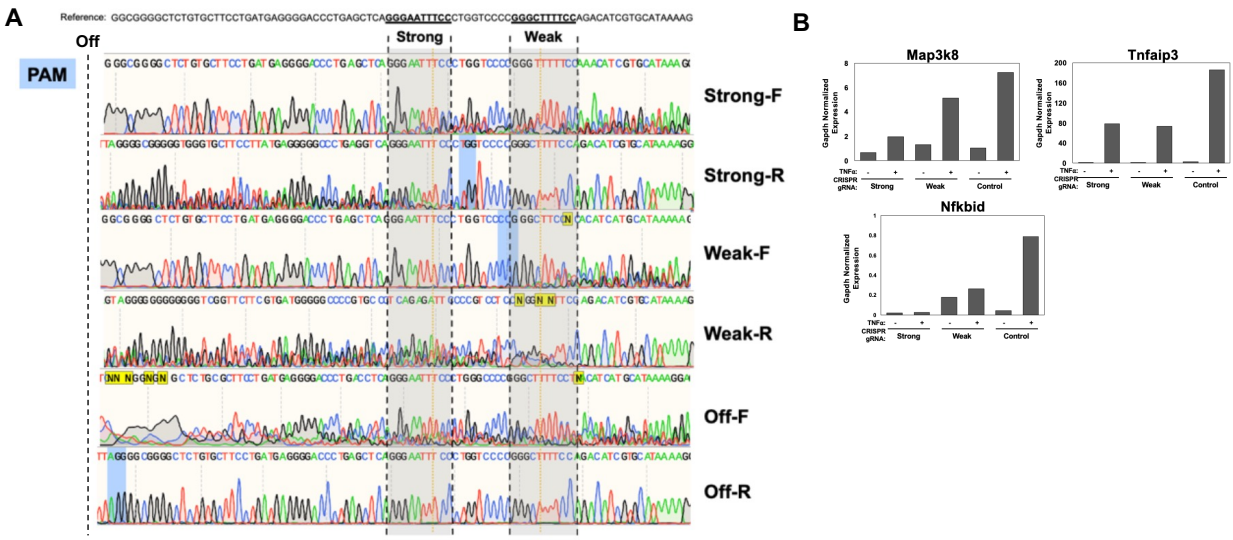

Supplementary Figure 2.
A. CRISPR-based mutagenesis of Cxcl2 promoter. The PAM sequences to generate the three mutants are shown by blue shades. Bulk cell DNA sequences of all three CRISPR targeted promoters are shown.
B. Transcript levels of Map3k8, Tnfaip3 and Nfkbid with their strong, weak, or a random site deleted by CRISPR in MEF cells upon TNFα stimulation at 1 h determined by RT-qPCR.

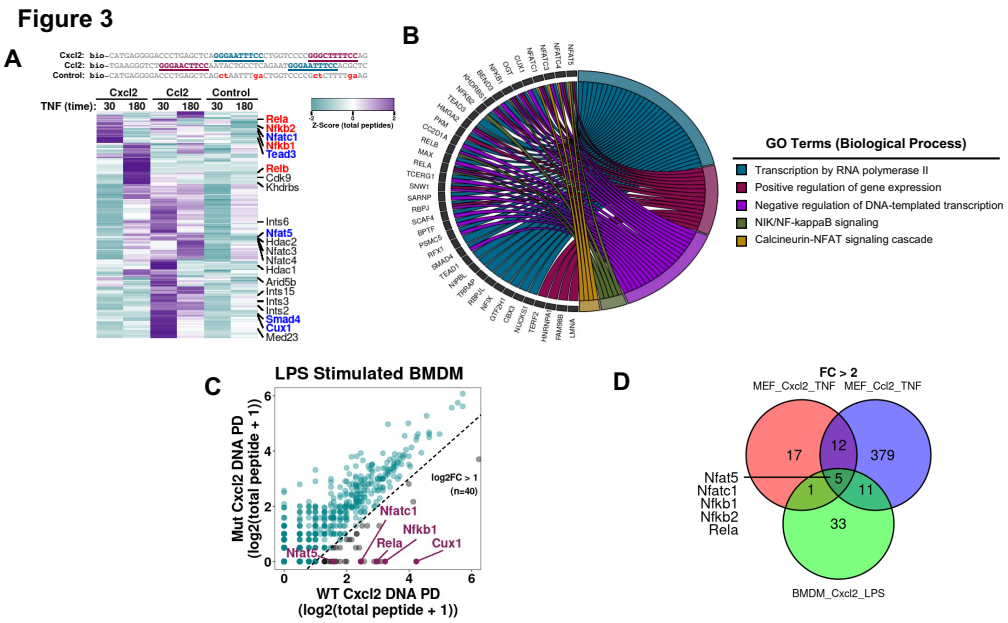

Figure 3. Association of a multitude of proteins with RelA-associated tandem κB sites adapted from Cxcl2 and Ccl2 promoters.

A. (Top) Sequence of DNA fragments used in pulldown experiments adapted from κB sites in promoter region of Cxcl2 and Ccl2 genes and a control DNA with no κB sites. (Bottom) Heat map displaying relative enrichment of proteins in TNFa-treated HeLa nuclear extracts bound to specific DNA compared to control DNA.

B. Biological pathway-specific classification of enriched proteins identified in A.

C. Correlation plot of total peptide counts from proteins identified by MS in LPS-treated BMDM nuclear extracts enriched by binding to Cxcl2 DNA fragment compared non-specific DNA.

D. A Venn diagram displaying commonality of cofactors from different cell types, DNA, and stimuli.

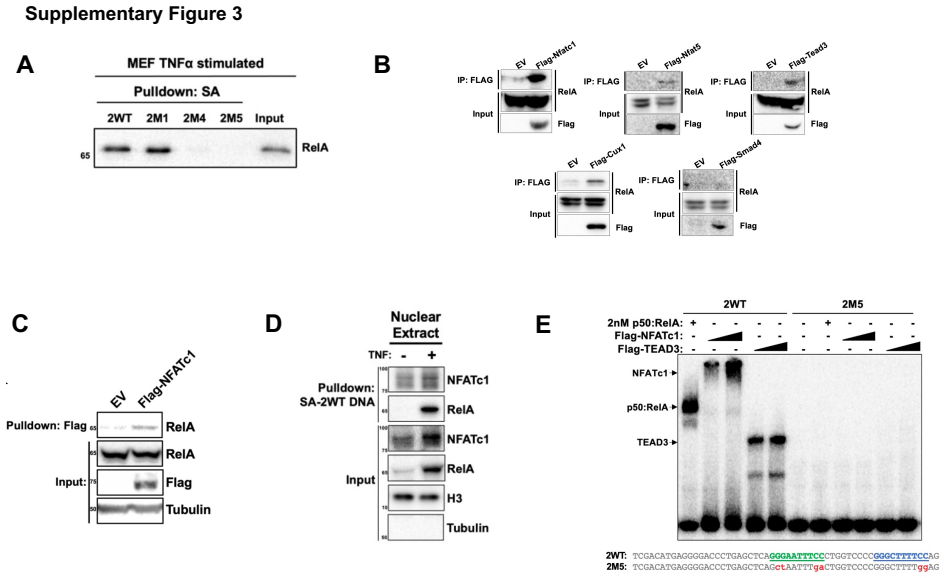

Supplementary Figure 3. Identification of cofactors, assessment of their activation, and their interactions with RelA in presence of κB DNA.
A. Pulldown from MEF nuclear extracts using biotinylated wild-type and mutant Cxcl2 DNAs indicating presence of RelA.
B. Flag pulldown of Flag-tagged Nfatc1, Nfat5, Tead3, Cux1, and Smad4 in TNFa-indcued HEK293T cotransfected with HA-tagged RelA.
C. Immunoprecipitation using anti-Flag beads and cell lysate of HEK293 cells transfected with Flag-tagged Nfatc1 with endogenous RelA.
D. Biotinylated DNA-streptavidin bead pulldown assay using wild-type Cxcl2 promoter DNA with control or TNFa stimulated MEF nuclear extract.
E. EMSA of Cxcl2 promoter DNA probes with purified recombinant p50:RelA heterodimer, Flag-NFATc1, and Flag-TEAD3.

Figure 4

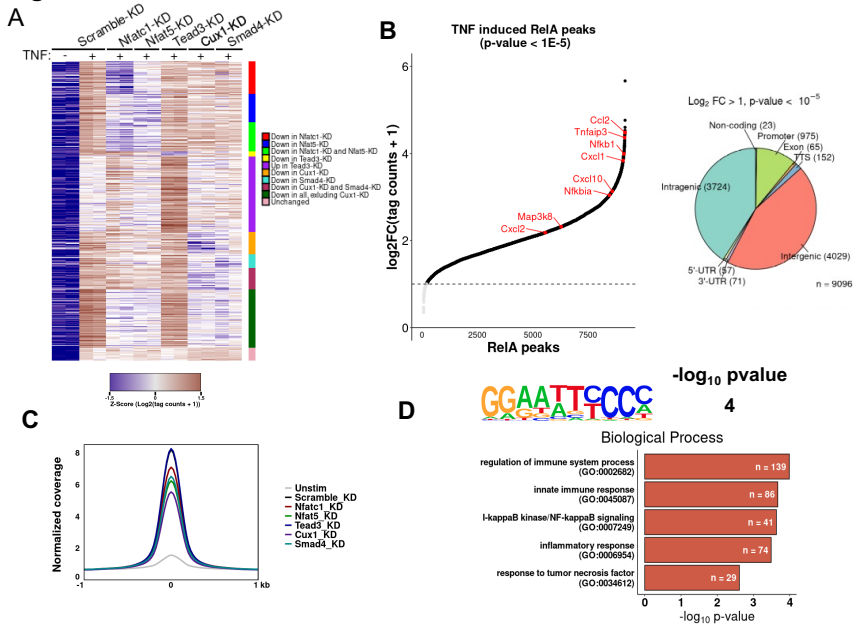

Figure 4. ChIP-seq showing regulation of NF-κB RelA recruitment by TF-cofactors.
A. RelA ChIP-seq comparison of different knockdown cell lines after 30 minutes of TNFa stimulation. Colors represent Z-score and categories of clustering are listed to right.
B. (Left) Induced RelA ChIP-seq binding represented as log2 fold change (log2FC) at the CRR of different RelA regulated genes in control cells after TNFa stimulation. Dotted line represents a log2 fold change cutoff of 1. (Right) Venn diagram representation of the location of ChIP-seq peaks at various genomic loci.
C. Relative peak strengths over all RelA peaks in knockdown cell lines.
D. (Top) Motif enrichment analysis identified the consensus κB sequence as the top motif identified. (Bottom) Gene ontology analysis of Biological Process pathways significantly enrichment in the genes with RelA-induced peaks.

Supplementary Figure 4

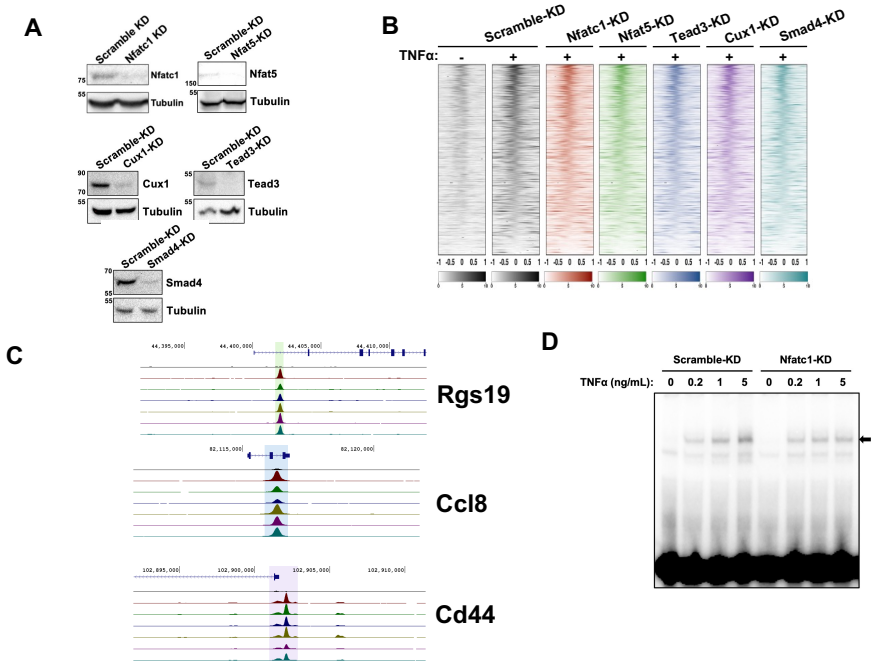

Supplementary Figure 4. RelA ChIP of control and five different KD MEF cell lines.
A. Western blot showing KD efficiencies.
B. Histogram representation of all RelA-induced peaks (log2FC > 1, p-value < 1E-5) across all cell lines upon TNFa stimulation.
C. Genome browser representation of RelA induced ChIP-Seq peaks across all knockdown cell lines to show variable effects of different knockdowns at the target genes Rgs19, Ccl8, and Cd44.
D. Cxcl2 (wild-type) promoter DNA binding activity of RelA is shown by EMSA of Scramble-KD and Nfatc1-KD MEF cells induced with increasing TNFa concentrations.

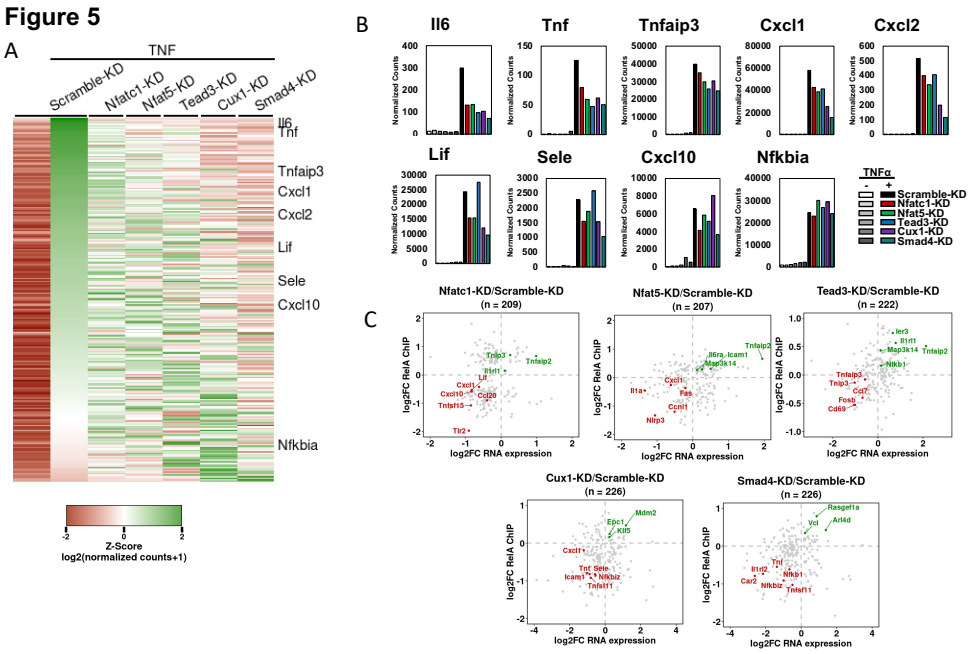

Figure 5. Transcriptomic analysis of various KD cells by RNA-seq in response to TNFa.
A. Heatmap representation of normalized read Z-scores of shared upregulated or downregulated genes in 7 different samples (average of n=3 in each case) (log2 fold-change > 0.5, p value < 0.01) from no or 1-hour TNFa stimulation. Genes are sorted with highest to lowest Z-scores in scrambled-KD stimulated samples. Genes are arranged accordingly for the rest of samples.
B. Expression of nine well-characterized RelA target under different KD conditions are presented as normalized counts.
C. ChIP-seq and RNA-seq correlation plot of TNFa-treated KD MEFs compared to scrambled-KD control cells.

Supplementary Figure 5

A

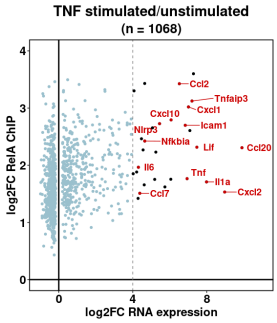

Supplementary Figure 5.
A. Correlation between induced RelA ChIP-Seq binding and in scramble-KD cells.

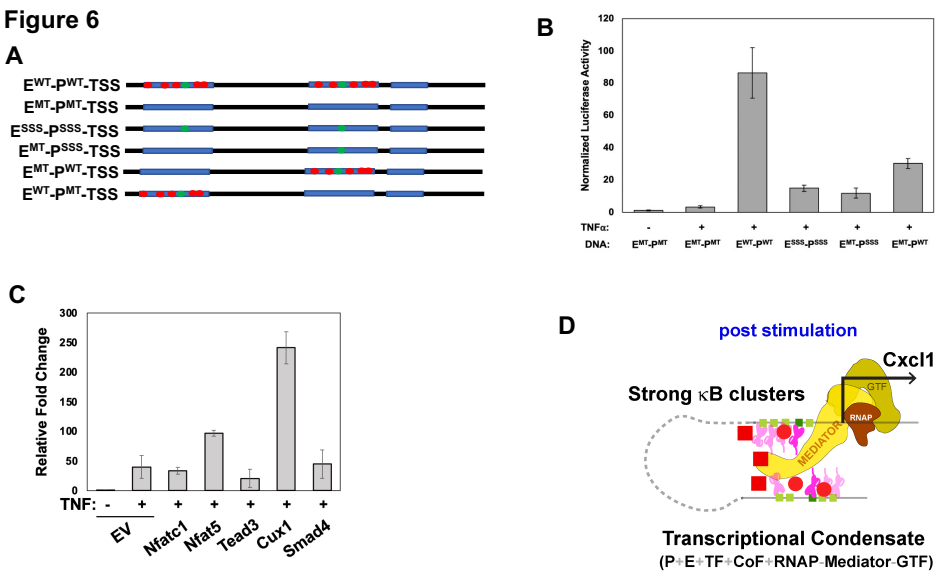

Figure 6. RelA forms transcriptional condensates with WT promoter and enhancers containing multiple weak sites and cofactors.
A. Cartoon showing reporter constructs of WT CRR with multiple κB sites each in the promoter and enhancer of Cxcl1 gene and various mutants. The enhancer and promoter are separated by 0.7 kb.
B. Normalized luciferase activity of transfected WT and mutant enhancer promoter combinations in 6 hour TNFa stimulated HeLa cells.
C. Normalized luciferase activity of E^{WT}-PW^{ET} in transfected HeLa cells cotransfected with Flag-tagged cofactors. Cells were stimulated for 6 hours with TNFa before harvesting.
D. A schematic of RelA transcription condensate formed at the Cxcl1 promoter site.

Supplementary Figure 6

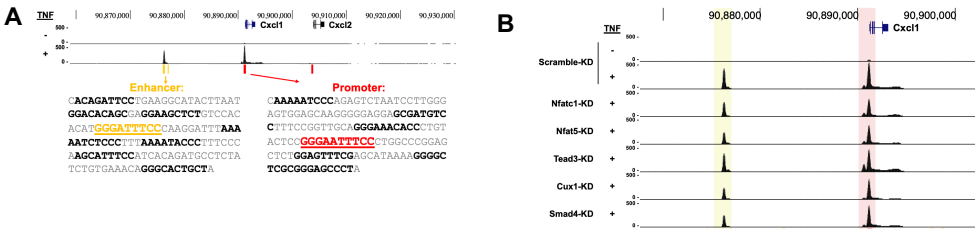

Supplementary Figure 6. Genomic organization of the Cxcl1 enhancer and promoter.
A. Genome browser representation at the Cxcl1 locus of RelA ChIP-Seq binding from 30 min TNFa stimulated control cells. Below tracks, yellow shows predicted enhancer and red shows predicted promoters from ENCODE database. Shown below are sequences of the enhancer and promoter, with putative weak signs shown in black and the central site colored.
E-P-TSS and RelA condensation in the presence of activated MEF NEs.
B. Genome browser representation displaying average RelA ChIP-Seq binding across replicates of knockdown cell lines following TNFa stimulation. Highlighted regions identity the enhancer (yellow) and promoter (red) of the Cxcl1 locus.

Figure 7

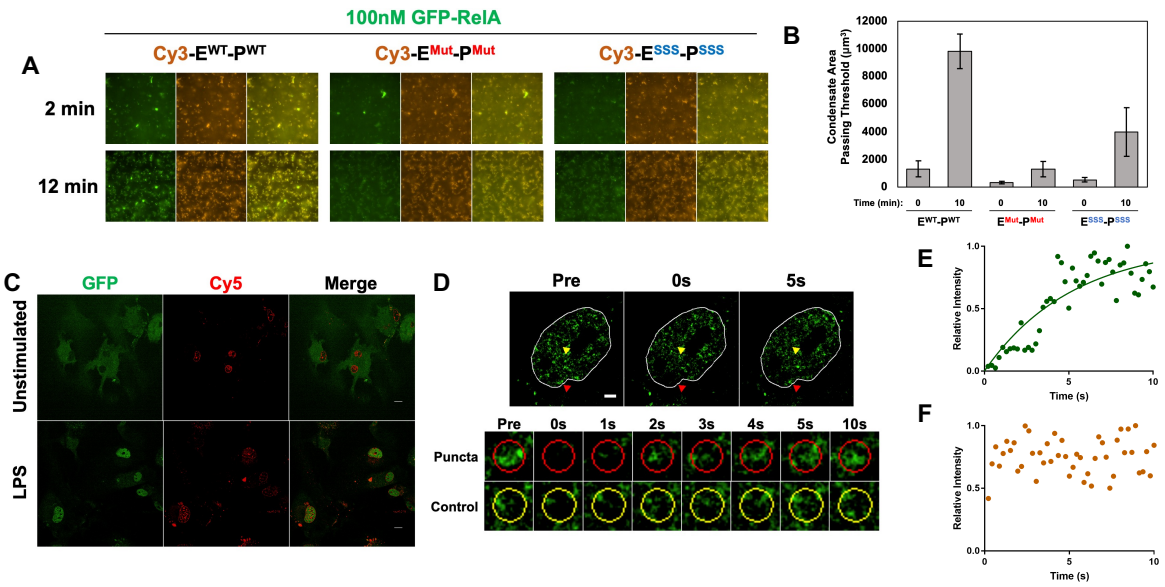

Figure 7. Clustered κB sites are essential to form transcriptional condensates.
A. Fluorescence microscopy images with 100x magnification of condensates formed with 100 nM GFP-RelA, 30 nM Cy3-DNA, and 1 mg/mL of TNFa stimulated HeLa nuclear extract at indicated timepoints.
B. Quantification of GFP-RelA condensate region covered per frame at indicated timepoints as shown in A.
C. Representative confocal microscopy images of mVenus-tagged RelA MEF before and after 1 hour LPS stimulation. (White scale = 10 μm.).
D. (top) Whole nuclear fluorescence microscopy image of mVenus RelA before (Pre), immediately following (0s), and after recovery (5s) of photobleaching at region denoted by red arrow. A control non-targeted region is denoted in yellow for analysis. (White scale = 2 μm) (bottom) Representative scaled microscopy images of region targeted for FRAP and control.
E. and **F.** Quantification of mVenus-RelA intensity throughout time course in puncta targeted (**E.**) and control (**F.**) regions.

Supplementary Figure 7

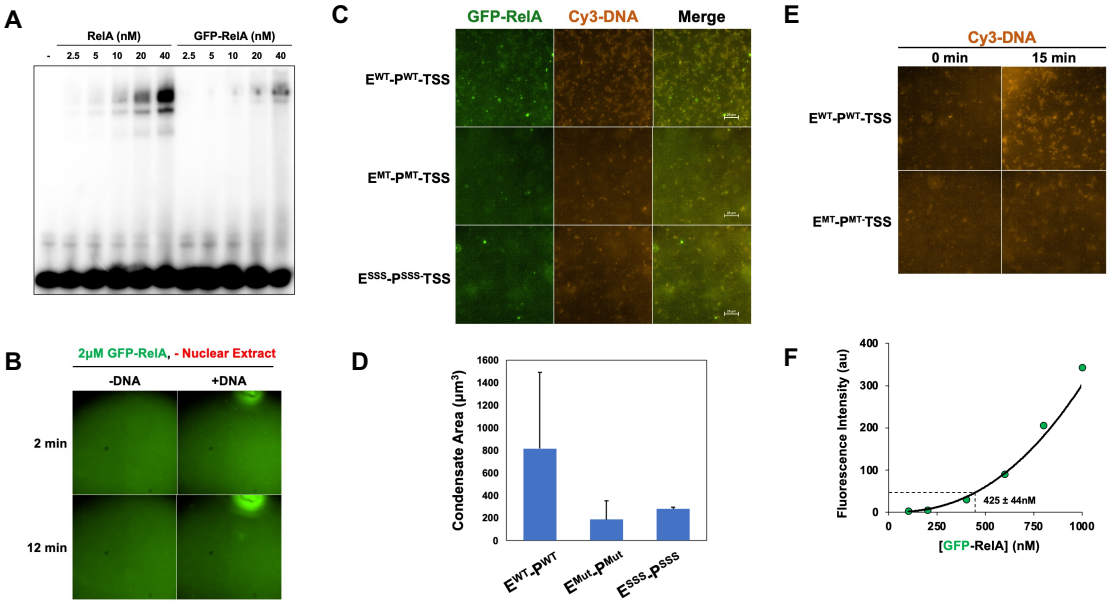

Supplementary Figure 7.

A. EMSA showing comparative DNA binding by wild-type RelA and RelA-GFP fusion homodimers expressed in and purified from the baculovirus expression system.

B. Fluorescence microscopy image of *in vitro* condensate assay in the absence of nuclear extract and with 2 μM GFP-RelA and Cy3-labeled E^{WT}-PW^{ET} DNA showing no RelA condensate formation.

C. Fluorescence microscopy images of condensates formed at center of droplet in different Cy3-labeled DNAs with 100 nM GFP-RelA and 1 mg/mL stimulated HeLa nuclear extract after 12 minutes of incubation.

D. Quantification of GFP-RelA condensate area covered from different frames in the middle of droplet as shown in **C.**

E. Fluorescence microscopy image of condensates formed in the absence of GFP-RelA with 1 mg/mL stimulated HeLa nuclear extract and Cy3-labeled DNAs.

F. Standard curve as a function of fluorescence intensity and GFP-RelA concentration in droplets. Concentrations of GFP-RelA used were 100, 200, 400, 600, 800, and 1000 nM and the concentration of GFP-RelA in the condensate was calculate to reach approximately 425 nM from a condensate assay with 100 nM GFP RelA after 12 minutes.

REFERENCES

Abe, Y., Kofman, E.R., Almeida, M., Ouyang, Z., Ponte, F., Mueller, J.R., Cruz-Becerra, G., Sakai, M., Prohaska, T.A., Spann, N.J., et al. (2023). RANK ligand converts the NCoR/HDAC3 co-repressor to a PGC1beta- and RNA-dependent co-activator of osteoclast gene expression. Molecular cell *83*, 3421-3437 e3411. 10.1016/j.molcel.2023.08.029.

Adelaja, A., Taylor, B., Sheu, K.M., Liu, Y., Luecke, S., and Hoffmann, A. (2021). Six distinct NFkappaB signaling codons convey discrete information to distinguish stimuli and enable appropriate macrophage responses. Immunity *54*, 916-930 e917. 10.1016/j.immuni.2021.04.011.

Badis, G., Berger, M.F., Philippakis, A.A., Talukder, S., Gehrke, A.R., Jaeger, S.A., Chan, E.T., Metzler, G., Vedenko, A., Chen, X., et al. (2009). Diversity and complexity in DNA recognition by transcription factors. Science (New York, N.Y.) *324*, 1720-1723. 10.1126/science.1162327.

Bosisio, D., Marazzi, I., Agresti, A., Shimizu, N., Bianchi, M.E., and Natoli, G. (2006). A hyper-dynamic equilibrium between promoter-bound and nucleoplasmic dimers controls NF-kappaB-dependent gene activity. The EMBO journal *25*, 798-810. 10.1038/sj.emboj.7600977.

Brignall, R., Moody, A.T., Mathew, S., and Gaudet, S. (2019). Considering Abundance, Affinity, and Binding Site Availability in the NF-kappaB Target Selection Puzzle. Front Immunol *10*, 609. 10.3389/fimmu.2019.00609.

Callegari, A., Sieben, C., Benke, A., Suter, D.M., Fierz, B., Mazza, D., and Manley, S. (2019). Single-molecule dynamics and genome-wide transcriptomics reveal that NF-kB (p65)-DNA binding times can be decoupled from transcriptional activation. PLoS Genet *15*, e1007891. 10.1371/journal.pgen.1007891.

Cheng, Q.J., Ohta, S., Sheu, K.M., Spreafico, R., Adelaja, A., Taylor, B., and Hoffmann, A. (2021). NF-kappaB dynamics determine the stimulus specificity of epigenomic reprogramming in macrophages. Science (New York, N.Y.) *372*, 1349-1353. 10.1126/science.abc0269.

Cho, W.K., Spille, J.H., Hecht, M., Lee, C., Li, C., Grube, V., and Cisse, II (2018). Mediator and RNA polymerase II clusters associate in transcription-dependent condensates. Science (New York, N.Y.) *361*, 412-415. 10.1126/science.aar4199.

Crocker, J., Abe, N., Rinaldi, L., McGregor, A.P., Frankel, N., Wang, S., Alsawadi, A., Valenti, P., Plaza, S., Payre, F., et al. (2015). Low affinity binding site clusters confer hox specificity and regulatory robustness. Cell *160*, 191-203. 10.1016/j.cell.2014.11.041.

Crocker, J., Noon, E.P., and Stern, D.L. (2016). The Soft Touch: Low-Affinity Transcription Factor Binding Sites in Development and Evolution. Curr Top Dev Biol *117*, 455-469. 10.1016/bs.ctdb.2015.11.018.

Farley, E.K., Olson, K.M., Zhang, W., Brandt, A.J., Rokhsar, D.S., and Levine, M.S. (2015). Suboptimization of developmental enhancers. Science (New York, N.Y.) *350*, 325-328. 10.1126/science.aac6948.

Farnung, L., and Vos, S.M. (2022). Assembly of RNA polymerase II transcription initiation complexes. Curr Opin Struct Biol *73*, 102335. 10.1016/j.sbi.2022.102335.

Fu, K., Sun, X., Zheng, W., Wier, E.M., Hodgson, A., Tran, D.Q., Richard, S., and Wan, F. (2013). Sam68 modulates the promoter specificity of NF-kappaB and mediates expression of CD25 in activated T cells. Nature communications *4*, 1909. 10.1038/ncomms2916.

Ghosh, G., Wang, V.Y., Huang, D.B., and Fusco, A. (2012). NF-kappaB regulation: lessons from structures. Immunological reviews *246*, 36-58. 10.1111/j.1600-065X.2012.01097.x.

Gordan, R., Hartemink, A.J., and Bulyk, M.L. (2009). Distinguishing direct versus indirect transcription factor-DNA interactions. Genome Res *19*, 2090-2100. 10.1101/gr.094144.109.

Hnisz, D., Shrinivas, K., Young, R.A., Chakraborty, A.K., and Sharp, P.A. (2017). A Phase Separation Model for Transcriptional Control. Cell *169*, 13-23. 10.1016/j.cell.2017.02.007.

Hudson, W.H., and Ortlund, E.A. (2014). The structure, function and evolution of proteins that bind DNA and RNA. Nat Rev Mol Cell Biol *15*, 749-760. 10.1038/nrm3884.

Kim, S., and Wysocka, J. (2023). Deciphering the multi-scale, quantitative cis-regulatory code. Molecular cell *83*, 373-392. 10.1016/j.molcel.2022.12.032.

Kribelbauer, J.F., Rastogi, C., Bussemaker, H.J., and Mann, R.S. (2019). Low-Affinity Binding Sites and the Transcription Factor Specificity Paradox in Eukaryotes. Annu Rev Cell Dev Biol *35*, 357-379. 10.1146/annurev-cellbio-100617-062719.
Lambert, S.A., Jolma, A., Campitelli, L.F., Das, P.K., Yin, Y., Albu, M., Chen, X., Taipale, J., Hughes, T.R., and Weirauch, M.T. (2018). The Human Transcription Factors. Cell *172*, 650-665. 10.1016/j.cell.2018.01.029.
Lenardo, M.J., and Baltimore, D. (1989). NF-kappa B: a pleiotropic mediator of inducible and tissue-specific gene control. Cell *58*, 227-229. 10.1016/0092-8674(89)90833-7.
Leung, T.H., Hoffmann, A., and Baltimore, D. (2004). One nucleotide in a kappaB site can determine cofactor specificity for NF-kappaB dimers. Cell *118*, 453-464. 10.1016/j.cell.2004.08.007.
Li, T., Shahabi, S., Biswas, T., Tsodikov, O.V., Pan, W., Huang, D.B., Wang, V.Y., Wang, Y., and Ghosh, G. (2024). Transient interactions modulate the affinity of NF-kappaB transcription factors for DNA. Proceedings of the National Academy of Sciences of the United States of America *121*, e2405555121. 10.1073/pnas.2405555121.
Lim, F., Solvason, J.J., Ryan, G.E., Le, S.H., Jindal, G.A., Steffen, P., Jandu, S.K., and Farley, E.K. (2024). Affinity-optimizing enhancer variants disrupt development. Nature *626*, 151-159. 10.1038/s41586-023-06922-8.
Lu, F., and Lionnet, T. (2021). Transcription Factor Dynamics. Cold Spring Harb Perspect Biol *13*. 10.1101/cshperspect.a040949.
Maul, G.G., and Deaven, L. (1977). Quantitative determination of nuclear pore complexes in cycling cells with differing DNA content. J Cell Biol *73*, 748-760. 10.1083/jcb.73.3.748.
Meeussen, J.V.W., and Lenstra, T.L. (2024). Time will tell: comparing timescales to gain insight into transcriptional bursting. Trends Genet *40*, 160-174. 10.1016/j.tig.2023.11.003.
Mulero, M.C., Huang, D.B., Nguyen, H.T., Wang, V.Y., Li, Y., Biswas, T., and Ghosh, G. (2017). DNA-binding affinity and transcriptional activity of the RelA homodimer of nuclear factor kappaB are not correlated. The Journal of biological chemistry *292*, 18821-18830. 10.1074/jbc.M117.813980.
Mulero, M.C., Shahabi, S., Ko, M.S., Schiffer, J.M., Huang, D.B., Wang, V.Y., Amaro, R.E., Huxford, T., and Ghosh, G. (2018). Protein Cofactors Are Essential for High-Affinity DNA Binding by the Nuclear Factor kappaB RelA Subunit. Biochemistry *57*, 2943-2957. 10.1021/acs.biochem.8b00158.
Mulero, M.C., Wang, V.Y., Huxford, T., and Ghosh, G. (2019). Genome reading by the NF-kappaB transcription factors. Nucleic acids research. 10.1093/nar/gkz739.
Ngo, K.A., Kishimoto, K., Davis-Turak, J., Pimplaskar, A., Cheng, Z., Spreafico, R., Chen, E.Y., Tam, A., Ghosh, G., Mitchell, S., and Hoffmann, A. (2020). Dissecting the Regulatory Strategies of NF-kappaB RelA Target Genes in the Inflammatory Response Reveals Differential Transactivation Logics. Cell Rep *30*, 2758-2775 e2756. 10.1016/j.celrep.2020.01.108.
Oksuz, O., Henninger, J.E., Warneford-Thomson, R., Zheng, M.M., Erb, H., Vancura, A., Overholt, K.J., Hawken, S.W., Banani, S.F., Lauman, R., et al. (2023). Transcription factors interact with RNA to regulate genes. Molecular cell *83*, 2449-2463 e2413. 10.1016/j.molcel.2023.06.012.
Sabari, B.R., Dall'Agnese, A., Boija, A., Klein, I.A., Coffey, E.L., Shrinivas, K., Abraham, B.J., Hannett, N.M., Zamudio, A.V., Manteiga, J.C., et al. (2018). Coactivator condensation at super-enhancers links phase separation and gene control. Science (New York, N.Y.) *361*. 10.1126/science.aar3958.
Scott, H.M., Smith, M.H., Coleman, A.K., Armijo, K.S., Chapman, M.J., Apostalo, S.L., Wagner, A.R., Watson, R.O., and Patrick, K.L. (2024). Serine/arginine-rich splicing factor 7 promotes the type I interferon response by activating Irf7 transcription. Cell Rep *43*, 113816. 10.1016/j.celrep.2024.113816.
Shrinivas, K., Sabari, B.R., Coffey, E.L., Klein, I.A., Boija, A., Zamudio, A.V., Schuijers, J., Hannett, N.M., Sharp, P.A., Young, R.A., and Chakraborty, A.K. (2019). Enhancer Features that Drive Formation of Transcriptional Condensates. Molecular cell *75*, 549-561 e547. 10.1016/j.molcel.2019.07.009.
Siggers, T., Chang, A.B., Teixeira, A., Wong, D., Williams, K.J., Ahmed, B., Ragoussis, J., Udalova, I.A., Smale, S.T., and Bulyk, M.L. (2011). Principles of dimer-specific gene regulation revealed by a comprehensive characterization of NF-kappaB family DNA binding. Nature immunology *13*, 95-102. 10.1038/ni.2151.
Todeschini, A.L., Georges, A., and Veitia, R.A. (2014). Transcription factors: specific DNA binding and specific gene regulation. Trends Genet *30*, 211-219. 10.1016/j.tig.2014.04.002.

Wan, F., Anderson, D.E., Barnitz, R.A., Snow, A., Bidere, N., Zheng, L., Hegde, V., Lam, L.T., Staudt, L.M., Levens, D., et al. (2007). Ribosomal protein S3: a KH domain subunit in NF-kappaB complexes that mediates selective gene regulation. Cell *131*, 927-939. 10.1016/j.cell.2007.10.009.
Wang, V.Y., Huang, W., Asagiri, M., Spann, N., Hoffmann, A., Glass, C., and Ghosh, G. (2012). The transcriptional specificity of NF-kappaB dimers is coded within the kappaB DNA response elements. Cell Rep *2*, 824-839. 10.1016/j.celrep.2012.08.042.
Xiao, R., Chen, J.Y., Liang, Z., Luo, D., Chen, G., Lu, Z.J., Chen, Y., Zhou, B., Li, H., Du, X., et al. (2019). Pervasive Chromatin-RNA Binding Protein Interactions Enable RNA-Based Regulation of Transcription. Cell *178*, 107-121 e118. 10.1016/j.cell.2019.06.001.
Zuin, J., Roth, G., Zhan, Y., Cramard, J., Redolfi, J., Piskadlo, E., Mach, P., Kryzhanovska, M., Tihanyi, G., Kohler, H., et al. (2022). Nonlinear control of transcription through enhancer-promoter interactions. Nature *604*, 571-577. 10.1038/s41586-022-04570-y.